

A CONSERVATIVE TWO-PHASE FLOW MODEL WITH A NONLINEAR DEGENERATE DIFFUSION

GLORIA FACCANONI^{1,*}, CÉDRIC GALUSINSKI¹ AND BÉRÉNICE GREC²

Abstract. This paper is motivated by the need to model the dynamics of liquid–vapor flows involving phase transitions in heat exchangers. In the low Mach number asymptotic limit, we derive a system of 1D conservation laws with heat transfers causing phase change, with a degenerate and nonlinear thermal diffusion coefficient. This degeneracy induces discontinuities on the solution, both on the enthalpy and the velocity. We provide explicit steady and travelling wave solutions, and derive suitable numerical schemes able to capture the moving discontinuities.

Mathematics Subject Classification. 35Q35, 35Q79, 65M25, 76T10.

Received April 4, 2025. Accepted November 15, 2025.

1. INTRODUCTION

The motivation for this study is to analyze the flow dynamics within a heat exchanger, typically in the core of a nuclear reactor [1]. We focus on a low Mach number model (LMNC model introduced in [2]), derived from a compressible model by letting the Mach number tend to zero. This approach allows to neglect acoustic waves, and simplifies greatly the equation of state, but retains the effects of large heat transfers. This approximation is relevant to describe the nominal regime in the core of a nuclear reactor, and even in some incidental situations.

A key aspect is to incorporate the liquid–gas phase change due to significant heat deposits [3, 4]. In our modeling, the fluid can exist either in a pure phase (liquid or vapor) or as a saturated mixture [5, 6]. Phase change was already introduced in the LMNC model without thermal diffusion in [7].

The originality of the model investigated in the present paper lies in considering thermal diffusion effects. Due to the diphasic nature of the flow, the thermal diffusion term is nonlinear and degenerates within the mixture, causing discontinuities in the solutions as the gas phase appears. Note that the discontinuity is related to the introduction of the degenerate thermal diffusion term, since without diffusion, the solution remains continuous even when the gas phase appears [7]. A first study without appearance of the gas phase was presented in [8]. Further works [9, 10] investigated the 1D steady-state solution for a simplified model assuming constant density and no velocity equation (constant velocity flow), and introduced an appropriate scheme. It was noted that this simplified LMNC model with degenerate thermal diffusion links diffuse interface models and Stefan problems (corresponding to sharp interfaces).

Keywords and phrases: Liquid–vapor phase transition, generalized Stefan problem, nonlinear degenerate diffusion, numerical schemes, discontinuity propagation.

¹ Université de Toulon – IMATH, EA 2134, 83957 La Garde, France.

² Université Paris Cité, CNRS, MAP5, F-75006 Paris, France.

* Corresponding author: gloria.faccanoni@univ-tln.fr

The original work of Stefan [11], formulated in terms of temperature, addressed the tracking of an interface during phase change. The literature on Stefan problems is huge and continually expanding, we refer to general monographies [12, 13]. Generalized Stefan problems extend the physics of sharp interfaces to the emergence of mushy regions (mixture of two phases), through a formulation in terms of enthalpy. This formulation leads to a nonlinear degenerate parabolic evolution equation, and has been extensively studied from the mathematical and numerical points of view (*cf.* the pioneering works [14, 15] and further mathematical references as [16, 17]). Such degenerate equations also arise in porous media, as in the Richards equation [18], presenting similar theoretical and numerical challenges. While the classical enthalpy-based Stefan model focuses on the thermodynamics of phase change, it does not account for hydrodynamic couplings. The objective of the present work is to study the coupling between hydrodynamic and thermodynamic effects during phase change.

The novelty of our study is to couple the energy equation with an equation on the velocity, so that neither velocity nor density are constant, and all quantities exhibit discontinuities at the gas phase boundary. The challenge of this model is to handle these discontinuities in both enthalpy and velocity. Because of these discontinuities, care must be taken to avoid developing non-conservative products, which is actually not the usual approach when dealing with a low Mach number asymptotic model. In particular, the velocity part of the model of Navier–Stokes type is often investigated under a non-conservative form with the constraint on the divergence of the velocity, and this cannot be applied here. This requires to revisit the analysis and numerical schemes developed in previous works. Besides, numerical difficulties arise to capture these singular solutions, and the highly coupled nature of the model limits the choice of appropriate discretization methods.

The article is structured as follows. In Section 2, we introduce the low Mach number model with thermal diffusion and phase change. We revisit in Section 3 the analytical solutions derived in [9] for the steady-state model. The novelty lies in a more direct approach of the proofs without relying on viscosity solutions. In Section 4, we propose a specific transient solution in the form of a travelling wave, and investigate the properties of the solutions. In Section 5, we introduce numerical schemes for solving the full time-dependent model. We begin by explaining why classical approaches for the LMNC model without thermal diffusion cannot be generalized, and then propose two suitable schemes for the model with thermal diffusion (one explicit based on a predictor-corrector approach, the other one fully implicit). In Section 6, we present numerical simulations for this model with thermal diffusion. We emphasize the numerical difficulties induced by the solution discontinuities and show that the proposed schemes capture these discontinuities.

2. A LOW MACH NUMBER MODEL FOR A HEAT EXCHANGER

This section introduces an adimensionalized low Mach number model designed specifically for a heat exchanger system, derived from the compressible Navier–Stokes–Fourier system. Since the analysis is done in 1D in the rest of the paper, we only describe the model in 1D, focusing on the main flow direction (which is vertical in the core of a nuclear reactor).

2.1. Governing equations

The asymptotic low Mach number model includes the conservation equations for mass, momentum, and energy, involving the following unknowns: the velocity $(t, y) \mapsto v$, the enthalpy $(t, y) \mapsto h$, and the dynamic pressure $(t, y) \mapsto \mathcal{P}$. The system is written as

$$\begin{cases} \partial_t \varrho(h) + \partial_y(\varrho(h)v) = 0, & (2.1a) \\ \partial_t(\varrho(h)v) + \partial_y(\varrho(h)v^2) + \partial_y \mathcal{P} = 0, & (2.1b) \\ \partial_t(\varrho(h)h) + \partial_y(\varrho(h)hv) = \Phi + \partial_{yy}(\mathcal{L}(h)). & (2.1c) \end{cases}$$

The full derivation of this model is presented in Appendix A. It is written in a non-dimensional form in system (A.13). In the whole paper, in order to focus on thermal effects, we neglect the viscous and the gravitational effects (this corresponds to choosing $\text{Fr}, \text{Re} \rightarrow \infty$). System (A.13) is then simplified to the previous system (2.1).

This model is closed by an equation of state, giving the density $h \mapsto \varrho(h)$ of the fluid. Observe that, contrary to the full compressible setting, the low Mach number asymptotic regime allows to simplify the thermodynamic equation of state, since it does not depend on the pressure and thus only depends on one variable h . The function $h \mapsto \mathcal{L}(h)$ is linked to the thermal diffusion coefficient (and also depends on h), and Φ is the power density modelling the heating (due to fission reactions in a nuclear reactor). For the sake of simplicity, $\Phi \geq 0$ is assumed to be constant.

Observe that even without thermal diffusion, the system (2.1) is not hyperbolic, which is intrinsic to the low Mach number asymptotic regime [7]. Indeed, in this setting, the velocity v can be seen as a Lagrange multiplier (which is obvious in the model written under a non-conservative form) in order to satisfy the two conservation equations depending on the same unknown, the enthalpy.

Observe that in 1D, the pressure \mathcal{P} can be solved separately from the other unknowns as a post-treatment by integrating the equation (2.1b)

$$\partial_y \mathcal{P} = -\partial_t(\varrho v) - \partial_y(\varrho v^2).$$

In the following, we will thus only focus on equations (2.1a) and (2.1c) for the unknowns v and h , closed with the equation of state $\varrho(h)$ and the determination of $\mathcal{L}(h)$.

In order to take into account phase transition phenomena, the equation of state for diphasic fluids is described in the following section.

2.2. Diphasic equation of state with phase transition

To complete the system, we have to describe the behavior of a compressible diphasic fluid undergoing possible phase transition. In a general compressible setting, describing a pure phase $\kappa \in \{\ell, g\}$ (liquid phase ℓ or a gas one g) requires to provide the equation of state $\varrho_\kappa(h, p)$ and $T_\kappa(h, p)$ (which appears in the thermal diffusion term). During phase change, a transitional area may appear at the interface of the two phases. Within this zone, the fluid is assumed to be at saturation (equilibrium) during phase transition. At saturation, both phases have identical pressure p , temperature T , and chemical potential \mathbf{g} . The saturation temperature $T^s(p)$ is defined from the thermodynamical relation $\mathbf{g}_\ell(T, p) = \mathbf{g}_g(T, p)$ (see [5, 6]). The transition between a pure phase to the mixture happens at the saturation enthalpy $h_\kappa^s(p) \stackrel{\text{def}}{=} h_\kappa(T^s(p), p)$ for each phase κ .

Specifically, at pressure p , the phase of the fluid is determined by its enthalpy h : it exists under the liquid phase if $h \leq h_\ell^s(p)$, under the gas phase if $h \geq h_g^s(p)$, and as a mixture at saturation when $h_\ell^s(p) < h < h_g^s(p)$. The density ϱ and the temperature T are then piecewise defined with respect to $h_\kappa^s(p)$:

$$\varrho(h, p) = \begin{cases} \varrho_\ell(h, p), & \text{if } h \leq h_\ell^s(p), \\ \varrho_m(h, p), & \text{if } h_\ell^s(p) < h < h_g^s(p), \\ \varrho_g(h, p), & \text{if } h \geq h_g^s(p), \end{cases} \quad T(h, p) = \begin{cases} T_\ell(h, p), & \text{if } h \leq h_\ell^s(p), \\ T^s(p), & \text{if } h_\ell^s(p) < h < h_g^s(p), \\ T_g(h, p), & \text{if } h \geq h_g^s(p). \end{cases}$$

The adimensionalization of the equation of state is described in Appendix A.

In our model, the thermodynamic quantities are evaluated at $p = p_*$, which is constant. The equation of state for ϱ then becomes

$$\varrho(h) = \begin{cases} \varrho_\ell(h) & \text{if } h \leq h_\ell^s, \\ \varrho_m(h) & \text{if } h_\ell^s < h < h_g^s, \\ \varrho_g(h) & \text{if } h \geq h_g^s. \end{cases} \quad (2.2)$$

In pure phases, the mixture density $\varrho_\kappa(h)$, $\kappa = \ell, g$ are given by the chose equation of state. However, in the mixture at saturation, the function ϱ_m has been computed in [19] (see the references therein for more details).

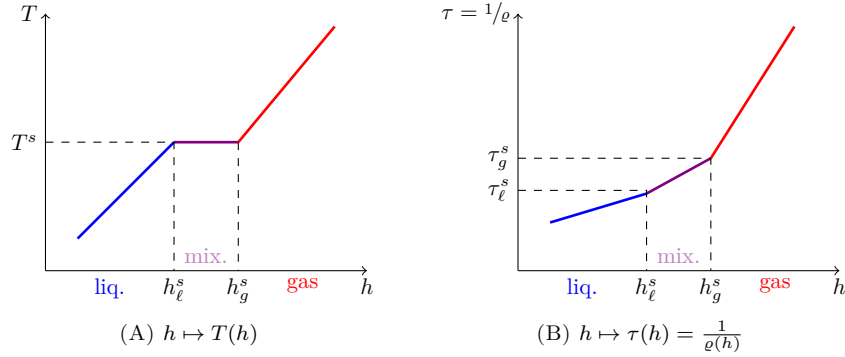


FIGURE 1. Temperature and specific volume at constant pressure.

It is proved that it always has the structure of a stiffened gas, and is given by

$$\varrho_m(h) = \frac{h - q_m}{\zeta_m},$$

where ζ_m and q_m are constants depending on the thermodynamic properties of the saturation.

Further, since the saturation temperature is constant, $T'(h)$ is zero if the enthalpy is between h_ℓ^s and h_g^s (see Fig. 1(A)), whereas it is non-zero in pure phases. Let us recall from Appendix A the definitions (A.10), (A.11) and (A.14). We then have

$$\mathcal{L}'(h) = \begin{cases} \lambda_\ell, & \text{if } h \leq h_\ell^s, \\ 0, & \text{if } h_\ell^s < h < h_g^s, \\ \lambda_g, & \text{if } h \geq h_g^s. \end{cases} \quad (2.3)$$

For the sake of simplicity, we will assume in the following that λ_κ is constant for each phase κ (which means that the heat conductivity and the isobar heat capacity are constant and isotropic for each pure phase).

2.3. The final model

Finally, we look for the solutions v and h of the following system

$$\begin{cases} \partial_t \varrho + \partial_y(\varrho v) = 0, \\ \partial_t(\varrho h) + \partial_y(\varrho h v) = \Phi + \partial_{yy}(\mathcal{L}(h)), \end{cases} \quad (2.4)$$

where the piecewise constant function $\mathcal{L}'(h)$ is defined in (2.3) and the piecewise continuous function $\varrho(h)$ is defined in (2.2).

The system is posed over the semi-infinite domain $y \in \mathbb{R}^+$ with the Dirichlet (injection) boundary conditions at $y = 0$:

$$v(t, 0) = v_e > 0 \quad \text{and} \quad h(t, 0) = h_e < h_\ell^s, \quad (2.5)$$

where the injection values v_e and h_e are both constant, and allow to define the entrance flow $D_e \stackrel{\text{def}}{=} v_e \varrho(h_e) > 0$. When y tends to infinity, the asymptotic behavior is set to be

$$\lim_{y \rightarrow +\infty} \partial_y h(t, y) = \frac{\Phi}{D_e}. \quad (2.6)$$

The system is supplemented with an initial condition on $h(0, y)$ and $v(0, y)$.

Remark 2.1. The choice of $h_e < h_\ell^s$ in the boundary condition (2.5) is made to illustrate a complete case with up to three phases (liquid–mixture–gas). It should be noted that the different results proved in the paper can be extended to $h_e > h_\ell^s$ very easily, it just limits the number of phases to two or one (mixture–gas or gas).

The boundary condition at infinity (2.6) is chosen in order to fit the stationary solution when $\lambda_g = 0$ and corresponds to non additional energy deposited at infinity when $\lambda_g > 0$.

Remark 2.2. This model is studied in a simplified setting in [9] assuming a constant density, leading to a classical structure of a generalized degenerate Stefan problem with transport, where discontinuous solutions have been exhibited. The analysis of such models is for example studied in [16] and the numerical analysis with finite volume schemes is performed in [17, 20, 21].

In this paper, with a variable density, we expect the solutions to be again discontinuous, so that the non-conservative form cannot be expanded. This imposes to remain with the structure of two conservation equations, where the velocity acts as a Lagrangian multiplier. In the different context of hyperbolic equations, such a structure can be found in [22, 23].

3. THE STEADY-STATE MODEL

In this section, we revisit the analytical solutions derived in [9] for the steady-state model. The novelty lies in Lemma 3.2, which allows for a more direct approach in the proofs, particularly without relying on the concept of viscosity solutions.

3.1. Steady-state solution

The stationary system is given by

$$\begin{cases} \partial_y(\varrho v) = 0, \\ \partial_y(\varrho v h) = \Phi + \partial_{yy}(\mathcal{L}(h)), \end{cases} \quad y \in [0; +\infty),$$

with the boundary conditions (2.5)–(2.6).

The first equation implies that $(\varrho v)(y) = D_e$ for all $y \in \mathbb{R}^+$, reducing the second equation to

$$D_e \partial_y h = \Phi + \partial_{yy}(\mathcal{L}(h)), \quad (3.1)$$

which is independent of $h \mapsto \varrho(h)$. The velocity is then obtained by $v(y) = D_e / \varrho(h(y))$.

For the sake of simplicity, we shall denote in the rest of this section the space derivative $\partial_y(\cdot)$ by $(\cdot)'$.

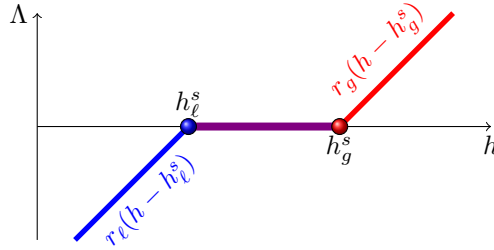
Let us introduce the following nonnegative constant ratios for $\kappa \in \{\ell, m, g\}$, and define the function $h \mapsto \Lambda(h)$ (see Fig. 2):

$$r_\kappa \stackrel{\text{def}}{=} \lambda_\kappa / D_e, \quad r_\Phi \stackrel{\text{def}}{=} \Phi / D_e, \quad h \mapsto \Lambda(h) = \mathcal{L}(h) / D_e. \quad (3.2)$$

The stationary model (3.1) is then rewritten as

$$h'(y) - (\Lambda(h))''(y) = r_\Phi, \quad y \in [0, +\infty), \quad (3.3)$$

and the asymptotic behavior as y approaches infinity is rewritten as $\lim_{y \rightarrow \infty} h'(y) = r_\Phi$.

FIGURE 2. $h \mapsto \Lambda(h)$.

To determine the phase at a given y , we compute the intersection points of the steady-state solution $y \mapsto h(y)$ with the two lines $h = h_\kappa^s$, $\kappa \in \{\ell, g\}$. These intersection points, marking the *phase transition points*, will be denoted by y_κ^s .

In the simple case $r_\ell = r_m = r_g = 0$, the model reduces to the stationary LMNC model without diffusion [7]. Its solution is restated in the following proposition for the sake of completion.

Proposition 3.1 (Solution without diffusion). *If $r_\ell = r_m = r_g = 0$, the steady-state solution for the enthalpy is continuous and given by $h(y) = h_e + r_\Phi y$.*

Proof. The equation becomes $h'(y) = r_\Phi$ with $h(0) = h_e$, which implies $h(y) = h_e + r_\Phi y$. \square

We will now focus on the model with a degenerate diffusion in the mixture at saturation, meaning that $r_m = 0$ and $r_\ell, r_g > 0$. In this case, the solution might present discontinuities. To investigate these possible discontinuities, let us introduce the notation $\llbracket h \rrbracket(y) = h(y^+) - h(y^-)$, and state the possible positions of discontinuities in the following lemma.

Lemma 3.2. *If $y \mapsto h(y)$ is an increasing function and if there exists a point $y_* \geq 0$ such that $\llbracket h \rrbracket(y_*) > 0$, then $\llbracket h \rrbracket(y_*) \leq h_g^s - h_\ell^s$ and $h(y_*^-) = h_\ell^s$ or $h(y_*^+) = h_g^s$.*

Proof. From the assumption $\llbracket h \rrbracket(y_*) > 0$, we know that h' contains a Dirac delta function δ_{y_*} at y_* , indicating that h' is a distribution of order 0.

Let us prove that $\llbracket \Lambda \circ h \rrbracket(y_*) = 0$ by contradiction. If $\llbracket \Lambda \circ h \rrbracket(y_*) > 0$, $(\Lambda \circ h)'$ also contains a Dirac delta function δ_{y_*} , implying that $(\Lambda \circ h)''$ is a distribution of order 1, which contradicts the equation.

Thus, since $\Lambda \circ h$ is continuous, $\Lambda(h(y_*^+)) = \Lambda(h(y_*^-))$. The form of Λ (see Fig. 2) implies that $h_\ell^s \leq h(y_*^-) < h(y_*^+) \leq h_g^s$, which means that the jump of h happens inside the mixture phase.

Let us now prove the conditions on y_* . Integrating the ODE $(h - (\Lambda \circ h))' = \Phi$, we find that $h - (\Lambda \circ h)$ is continuous, ensuring $\llbracket (\Lambda \circ h)' \rrbracket(y_*) = \llbracket h \rrbracket(y_*) > 0$. The form of Λ (see Fig. 2) implies that one of the extremities of the jump of h is located either at h_ℓ^s or h_g^s . Since the jump happens in the mixture phase, we thus deduce $h(y_*^-) = h_\ell^s$ or $h(y_*^+) = h_g^s$. \square

If the case of degenerate diffusion, two distinct scenarios emerge: a solution involving three regions (liquid/mixture/gas), or one with only two regions (liquid/gas) for the case when the mixture zone disappears. We shall see that the determination between these scenarios depends on the sign of $r_g r_\Phi - (h_g^s - h_\ell^s)$.

3.1.1. Case $r_g r_\Phi < h_g^s - h_\ell^s$: coexistence of the three phases (liquid/mixture/gas)

In the following proposition, we state the analytical solution in the case when the mixture region is present. We shall prove that the solution is continuous at the liquid/mixture transition, whereas it exhibits a discontinuity at a mixture/gas transition point.

Proposition 3.3. *If $r_g r_\Phi < h_g^s - h_\ell^s$, the mixture zone is present and the unique solution of (3.3) is discontinuous at y_g^s . It is given by the following expression*

$$h(y) = \begin{cases} h_\ell(y) \stackrel{\text{def}}{=} h_\ell^s + r_\Phi(y - y_\ell^s) + r_\ell r_\Phi \left(1 - \exp\left(\frac{y - y_\ell^s}{r_\ell}\right)\right) & \text{if } y \leq y_\ell^s, \\ h_m(y) \stackrel{\text{def}}{=} h_\ell^s + r_\Phi(y - y_\ell^s) & \text{if } y_\ell^s \leq y < y_g^s, \\ h_g(y) \stackrel{\text{def}}{=} h_g^s + r_\Phi(y - y_g^s) & \text{if } y \geq y_g^s. \end{cases} \quad (3.4)$$

The position y_ℓ^s of the liquid/mixture transition is implicitly defined by

$$r_\ell r_\Phi \left(1 - \exp\left(-\frac{y_\ell^s}{r_\ell}\right)\right) = h_e - h_\ell^s + y_\ell^s r_\Phi, \quad (3.5)$$

and the position y_g^s of the mixture/gas transition is computed w.r.t. y_ℓ^s by

$$y_g^s = y_\ell^s + \frac{h_g^s - h_\ell^s}{r_\Phi} - r_g. \quad (3.6)$$

Proof. We construct the solution starting from $y = 0$ (in the liquid phase, since we assumed $h_e < h_\ell^s$).

- *Pure liquid region.* The solution of the equation $h'_\ell(y) - r_\ell h''_\ell(y) = r_\Phi$ is given by $h_\ell(y) = A + r_\Phi y + B \exp(y/r_\ell)$. The boundary condition $h_\ell(0) = h_e$ results in $A = h_e - B$.

Let us now prove that, given $r_\Phi > 0$, the function $y \mapsto h_\ell(y)$ is an increasing function and that there is appearance of mixture, meaning that h_ℓ reaches the value h_ℓ^s at some point. We have

$$h'_\ell(y) = r_\Phi + \frac{B}{r_\ell} \exp\left(\frac{y}{r_\ell}\right), \quad h''_\ell(y) = \frac{B}{r_\ell^2} \exp\left(\frac{y}{r_\ell}\right).$$

If $B \geq 0$, h_ℓ is an increasing function and $h_\ell(y) \geq A + r_\Phi y$, thus it intersects the plateau $y = h_\ell^s$.

If $B < 0$, h_ℓ is increasing only on the interval $[0; r_\ell \ln(-\frac{r_\Phi r_\ell}{B})]$, if it exists. Therefore, the function h_ℓ is increasing only if it is so at $y = 0$ and if the liquid phase stops existing and the mixture phase appears, meaning that h_ℓ reaches the value h_ℓ^s at some point. Let us prove by contradiction that there exists a point $y_\ell^s > 0$ such that $h(y_\ell^s) = h_\ell^s$. If h did not reach h_ℓ^s , then $h_\ell(y)$ would be defined over the entire domain, but this contradicts the boundary condition on the right $\lim_{y \rightarrow \infty} h'(y) = r_\Phi > 0$.

At this point, we still need to determine the constant B as well as the position of the transition point y_ℓ^s . A first relation comes from the fact that $h(y_\ell^s) = h_\ell^s$ (linking B and y_ℓ^s), and another one is still missing and will be obtained by considering the jump condition in the mixture region at y_ℓ^s . Explicit computations of the constants will then be given.

- *Mixture region.* In the mixture region, solving $h'_m(y) = r_\Phi$ leads to $h_m(y) = C_m + r_\Phi y$. The function h_m is thus obviously increasing.

At the transition from the liquid to the mixture region, *i.e.* at y_ℓ^s , the jump relation yields

$$\underbrace{[[h]](y_\ell^s)}_{\geq 0} - 0 \times h'(y_\ell^{s,+}) + \underbrace{r_\ell h'(y_\ell^{s,-})}_{\geq 0} = 0,$$

which implies both $[[h]](y_\ell^s) = 0$ and $h'(y_\ell^{s,-}) = 0$.

The second relation allows to determine the constant B . Actually, it is more convenient to write the solution h_ℓ with respect to the point y_ℓ^s under the form

$$h_\ell(y) = C_{\ell,1} + r_\Phi(y - y_\ell^s) + C_{\ell,2} \exp((y - y_\ell^s)/r_\ell).$$

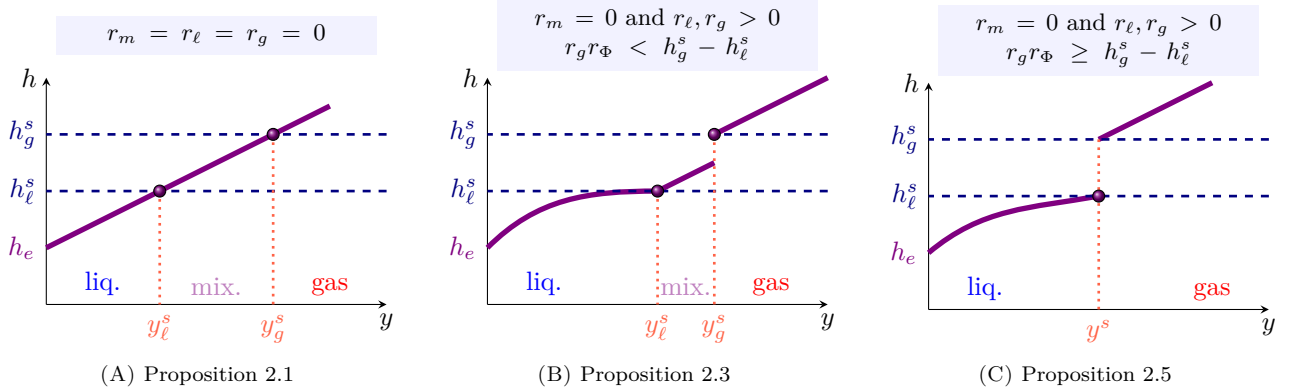


FIGURE 3. Sketch of the steady-state solution with and without thermal diffusion.

The conditions $h_\ell(y_\ell^s) = h_\ell^s$ and $h'_\ell(y_\ell^s) = 0$ immediately lead to $C_{\ell,1} = h_\ell^s + r_\ell r_\Phi$ and $C_{\ell,2} = -r_\ell r_\Phi$. Moreover, the condition $h_\ell(0) = h_e$ determines implicitly the position y_ℓ^s .

Further, the first relation implies that the solution is continuous at y_ℓ^s . Thus, $h_m(y_\ell^s) = h_\ell^s$, from which $C_m = h_\ell^s - r_\Phi y_\ell^s$.

Moreover, since h_m is increasing, there exists a point y_g^s such that $h_m(y_g^s) = h_g^s$: there is appearance of the gas phase.

- *Pure gas region.* Within the pure gas region, the solution of $h'_g(y) - r_g h''_g(y) = r_\Phi$ is given by $h_g(y) = C_{g,1} + r_\Phi(y - y_g^s) + C_{g,2} \exp((y - y_g^s)/r_g)$. From the boundary condition $\lim_{y \rightarrow \infty} h'_g(y) = r_\Phi$, it results that $C_{g,2} = 0$, thus $h_g(y) = C_{g,1} + r_\Phi(y - y_g^s)$ and $h'_g(y) = r_\Phi$.

Further, at the transition from the mixture to the gas region, the jump relation at y_g^s is

$$[[h]](y_g^s) - r_g h'(y_g^{s,+}) + 0 \times h'(y_g^{s,-}) = 0.$$

This implies that $[[h]](y_g^s) = r_g r_\Phi > 0$. Lemma 3.2 indicates that $h(y_g^{s,+}) = h_g^s$ and consequently $h_m(y_g^{s,-}) = h_g^s - r_g r_\Phi$. Since $h_m(y_g^{s,-}) = h_\ell^s + r_\Phi(y_g^s - y_\ell^s)$, we deduce that $y_g^s = y_\ell^s + \frac{h_g^s - h_\ell^s}{r_\Phi} - r_g$. In the gas, $h_g(y_g^s) = h_g^s = C_{g,1}$ so that $h_g(y) = h_g^s + r_\Phi(y - y_g^s)$. □

Remark 3.4 (Existence of the mixture region). From the expression of y_g^s given by (3.6), we can see that the gas diffusion coefficient $r_g > 0$ decreases the size of the mixture region with respect to the case without diffusion (*cf.* Figures 3(A) and 3(B)). It is expressed as $(y_g^s - y_\ell^s) = (\tilde{y}_g^s - \tilde{y}_\ell^s) - r_g$, where we denoted by $\tilde{y}_\kappa^s = (h_\kappa^s - h_e)/r_\Phi$ the location of the phase transition points without thermal diffusion (given by Prop. 3.1).

In particular, when $r_g r_\Phi = h_g^s - h_\ell^s$, we have $y_\ell^s = y_g^s$ and the value at the bottom of the jump is $h_m(y_g^{s,-}) = h_\ell^s$. The mixture zone disappears (*cf.* Figure 3(C)). Indeed, the jump relation at the mixture/gas transition point gives

$$[[h]](y_g^s) = h_g^s - h_m(y_g^s) = r_g r_\Phi,$$

which is exactly $h_g^s - h_\ell^s$ under the condition we mentioned. This establishes a transition from a diffusive interface model to a sharp interface model. This is the case we will consider in the next paragraph.

3.1.2. Case $r_g r_\Phi \geq h_g^s - h_\ell^s$: disappearance of mixture (transition liquid/gas)

In the following proposition, we state the analytical solution in the case when the mixture region disappears. The solution displays a discontinuity at the liquid/gas transition point.

Proposition 3.5. *If $r_g r_\Phi \geq h_g^s - h_\ell^s$, the mixture zone is not present and the unique solution of (3.3) is discontinuous. It is given by the following expression*

$$h(y) = \begin{cases} h_\ell(y) \stackrel{\text{def}}{=} h_\ell^s + r_\Phi(y - y^s) + ((r_\ell - r_g)r_\Phi + (h_g^s - h_\ell^s)) \left(1 - \exp\left(\frac{y - y^s}{r_\ell}\right)\right) & \text{if } y \leq y^s, \\ h_g(y) \stackrel{\text{def}}{=} h_g^s + r_\Phi(y - y^s) & \text{if } y \geq y^s. \end{cases} \quad (3.7)$$

The position y^s of the liquid/gas transition is implicitly defined by

$$(h_g^s - h_\ell^s + (r_\ell - r_g)r_\Phi) \left(1 - \exp\left(-\frac{y^s}{r_\ell}\right)\right) = h_e - h_\ell^s + y^s r_\Phi.$$

Proof. We construct again the solution starting from $y = 0$ (in the liquid phase by assumption $h_e < h_\ell^s$).

- *Pure liquid region.* With the same arguments as in the previous proposition, the solution in the liquid phase h_ℓ reaches the value h_ℓ^s at some point y^s , meaning that we have a phase transition, and it is given under the form $h_\ell(y) = C_{\ell,1} + r_\Phi(y - y^s) + C_{\ell,2} \exp((y - y^s)/r_\ell)$. The value at the transition point $h_\ell(y^s) = h_\ell^s$ determines the relation $C_{\ell,1} + C_{\ell,2} = h_\ell^s$ between the constants.
- *Non existence of the mixture region and transition liquid/gas.* As stated in Remark 3.4, the mixture zone disappears under the condition $r_g r_\Phi \geq h_g^s - h_\ell^s$. Therefore, the solution is discontinuous and we have a liquid/gas transition point at y^s .

The direct transition between liquid and gas phases represents a classic Stefan problem. As a result of Lemma 3.2, the jump is equal to $h_g^s - h_\ell^s$ and thus, in the vapor region, $h_g(y^s) = h_g^s$.

- *Pure gas region.* Within the pure gas region, the solution of $h'_g(y) - r_g h''_g(y) = r_\Phi$ is given by $h_g(y) = C_{g,1} + r_\Phi(y - y_g^s) + C_{g,2} \exp((y - y_g^s)/r_g)$. From the boundary condition $\lim_{y \rightarrow \infty} h'_g(y) = r_\Phi$, it results that $C_{g,2} = 0$, thus $h_g(y) = C_{g,1} + r_\Phi(y - y_g^s)$ and $h'_g(y) = r_\Phi$. The value at the transition point $h_g(y^s) = h_g^s$ determines the constant $C_{g,1} = h_g^s$.

Further, at the transition from the liquid to the gas region, the jump relation at y^s is

$$[[h]](y^s) = h_g^s - h_\ell^s = r_g h'_g(y^s) - r_\ell h'_\ell(y^s) = r_g r_\Phi - r_\ell r_\Phi - r_\ell \frac{C_{\ell,2}}{r_g}.$$

This leads the expression of $C_{\ell,2}$.

Finally, the expression of y^s is obtained by the boundary condition $h_\ell(0) = h_e$.

□

Remark 3.6. Observe that in the case when the mixture is present, $h'_\ell(y_\ell^s) = 0$, whereas when there is no mixture,

$$h'_\ell(y^s) = \frac{r_g r_\Phi - (h_g^s - h_\ell^s)}{r_\ell}$$

which is always positive and tends to $+\infty$ when $r_\ell \rightarrow 0$.

Remark 3.7. For the steady equation, two types of ratios appear: one between the diffusion and advection effects (r_ℓ and r_g), the other between the energy deposition and the flow rate (r_Φ). The product between the

ratios r_g and r_Φ determines the existence or not of the mixture region when compared to the difference between the saturation enthalpies of the liquid and gas phases.

Remark 3.8. Note that the discontinuity of the solution is a consequence of the degeneracy of the diffusion coefficient in the mixture region. Indeed, if we consider a non-degenerate diffusion coefficient $r_m > 0$ in the mixture region, the solution is continuous. Further, if the diffusion coefficient did not depend on h (but could degenerate with y), the solution would also be continuous.

Moreover, observe that when $r_\ell, r_g \rightarrow 0$, we are in the case of Subsection 3.1.1 and the solution given by Proposition 3.3 converges to the solution given by Proposition 3.1. Indeed, combining (3.4) with the expressions of y_ℓ^s and y_g^s given by (3.5) leads to $h(y) = h_e + r_\Phi y$ for all y when $r_\ell, r_g \rightarrow 0$.

To conclude, in models without diffusion, the presence of the mixture zone, *i.e.* a diffuse interface, always exists. However, the introduction of thermal diffusion modifies this zone. It reduces the extent of the mixture zone and generates a jump on the enthalpy at the mixture/gas transition. Negligible impact is observed when the thermal diffusion within the gas phase is small ($r_g r_\Phi \ll h_g^s - h_\ell^s$), which is the case in the core of a pressurized water reactor (*cf.* Appendix C). Conversely, under specific conditions ($r_g r_\Phi > h_g^s - h_\ell^s$), this reduction leads to its complete elimination, resulting in a steady state model characterized by a sharp interface.

This observation establishes a link to Stefan problems, which are discussed in the following subsection.

3.2. Link to the stationary Stefan problem

Stefan problems are one of the most fundamental frameworks to capture phase change processes. The stationary Stefan problem is a free boundary problem that can be expressed in enthalpy or temperature. In the formulation in temperature, the objective is to find y^s that meets the following conditions:

$$\begin{cases} c_{p,\ell} D_e T' - \omega_\ell T'' = \Phi \\ T(0) = T_e < T^s, \\ T(y^{s,-}) = T^s, \end{cases} \quad \text{in }]0, y^s[, \quad \begin{cases} c_{p,g} D_e T' - \omega_g T'' = \Phi \\ T(y^{s,+}) = T^s, \\ \lim_{y \rightarrow \infty} T'(y) = \frac{\Phi}{c_{p,g} D_e}, \end{cases} \quad \text{in }]y^s, +\infty[,$$

with the interface condition $\omega_g T'(y^{s,+}) - \omega_\ell T'(y^{s,-}) = D_e (h_g^s - h_\ell^s)$.

In this formulation, it is notable that when $r_g r_\Phi < h_g^s - h_\ell^s$ (indicating the presence of a “mushy” region according to our model), *i.e.* when $(\omega_g \Phi) / (c_{p,g} D_e) < D_e (h_g^s - h_\ell^s)$, the solution derived from the Stefan problem becomes non-physical. Specifically, the relation at the interface leads to

$$\omega_\ell T'(y^{s,-}) = \omega_g \frac{\Phi}{c_{p,g} D_e} - D_e (h_g^s - h_\ell^s) < 0,$$

which is inconsistent near y^s within the liquid phase, since this leads to temperatures decreasing to T^s , thus surpassing T^s .

Let us now discuss the enthalpy-based formulation. First, the classical Stefan problem assumes a sharp interface (forbidding any mixture between phases) with an enthalpy jump equals to the difference between saturated enthalpies $h_g^s - h_\ell^s$. Further, generalized Stefan problems were introduced, in which an intermediate “mushy” region between phases exist, as in our model. We computed that the jump is equal to the minimum value between $r_g r_\Phi$ and $h_g^s - h_\ell^s$ (and thus, our model coincides with the classical Stefan problem if $r_g r_\Phi \geq h_g^s - h_\ell^s$).

Having thoroughly examined the steady-state solution, the subsequent section focuses on the analysis of the time-dependent model.

4. TIME-DEPENDENT MODEL

In this section, we will describe some analytical properties of the solutions of the time-dependent model (2.4). We will describe the jump relations at the transition points, and present explicit travelling wave solutions.

4.1. Dynamic jump relations

Let us first state the possible jump relations, which will in particular have to be correctly approximated in suitable numerical schemes.

Proposition 4.1. *If the enthalpy is increasing and admits a limit from the left and a limit from the right at the transition point, then the jump relations at the possible mixture–gas and liquid–gas transitions are given by the following relations.*

- Mixture–gas transition. Assume that there exists a transition point $y_g^s(t)$ such that $h(y_g^{s,-}(t)) \in [h_\ell^s; h_g^s]$ and $h(y_g^{s,+}(t)) \geq h_g^s$. Then, the jump relations at the transition point are written

$$\begin{cases} 0 = -c(t)[[\varrho]](y_g^s(t)) + [[\varrho v]](y_g^s(t)) \\ 0 = -c(t)[[\varrho h]](y_g^s(t)) + [[\varrho h v]](y_g^s(t)) - \lambda_g(\partial_y h)(y_g^{s,+}(t)) \end{cases} \quad (4.1)$$

where we defined $c(t) \stackrel{\text{def}}{=} (y_g^s)'(t)$ the velocity of the gas interface.

- Liquid–gas transition. Assume that there exists a transition point $y^s(t)$ such that $h(y^{s,-}(t)) \leq h_\ell^s$ and $h(y^{s,+}(t)) \geq h_g^s$. Then, the jump relations at the transition point are written

$$\begin{cases} 0 = -c(t)[[\varrho]](y^s(t)) + [[\varrho v]](y^s(t)) \\ 0 = -c(t)[[\varrho h]](y^s(t)) + [[\varrho h v]](y^s(t)) + \lambda_\ell(\partial_y h)(y^{s,-}(t)) - \lambda_g(\partial_y h)(y^{s,+}(t)). \end{cases} \quad (4.2)$$

Proof. These jump relations are easily deduced from the conservative formulation (2.4) and the definition (2.3) of \mathcal{L} . \square

4.2. Analytical travelling wave

Here, we exhibit a travelling wave solution, which is increasing and linear within the mixture (if present) and the gas, akin to the stationary solution presented in Section 3. Such an analytical solution will be used for validation of numerical schemes. This solution relies on a stationary solution defined in the following lemma.

Lemma 4.2. *For any constant $K > 0$, let us define $r_\kappa \stackrel{\text{def}}{=} \lambda_\kappa/K$ and $r_\Phi \stackrel{\text{def}}{=} \Phi/K$. The solution of the stationary equation*

$$\begin{cases} \partial_y h - \partial_{yy} \frac{\mathcal{L}(h)}{K} = r_\Phi \\ h(0) = h_e \\ \lim_{y \rightarrow +\infty} h(y) = r_g r_\Phi \end{cases}$$

is given by (3.4) if $r_g r_\Phi < h_g^s - h_\ell^s$, and by (3.7) otherwise.

Proof. It is an immediate corollary of Proposition 3.3 and Proposition 3.5, with K instead of D_e . \square

Proposition 4.3. *Let $K > 0$ and $h_0(y)$ be a solution of the stationary problem given by Lemma 4.2. For any $c < 0$, the only travelling wave solution with velocity c of the system (2.4) with the initial conditions h_0 and $v_0(y) = c + K/\varrho(h_0(y))$ and the boundary inlet conditions $h_e(t) = h_0(-ct)$ and $v_e(t) = c + K/\varrho(h_e(t))$ is given by*

$$h(t, y) = h_0(y - ct) \quad \text{and} \quad v(t, y) = c + K/\varrho(h(t, y)).$$

Proof. Let $\rho(t, y) = \varrho(h(t, y))$. Looking for a travelling profile under the form $\rho(t, y) = \rho_0(y - ct)$, we have $\partial_t \rho = -c \partial_y \rho$, thus the first equation of the system (2.4) becomes $-c \partial_y \rho + \partial_y(\rho v) = 0$, meaning that $\partial_y((v - c)\rho) = 0$.

Therefore, the quantity $(v - c)\rho$ is constant and denoted by K , which leads to $v = c + K/\rho$. Further, the travelling wave profile for ρh also gives

$$\partial_y((v - c)\rho h) = [\Phi + \partial_{yy}\mathcal{L}(h)],$$

so that the equation reduces to

$$K\partial_y h - \partial_{yy}\mathcal{L}(h) = \Phi.$$

Applying Lemma 4.2, we deduce that the solution h is given either by (3.4) or by (3.7). □

Remark 4.4. Observe that the transition points (either $y_\ell^s(t)$ and $y_g^s(t)$, or $y^s(t)$) depend on t since $h_e(t)$ is not constant.

Remark 4.5. Note that the travelling waves exhibited here are the only ones that can be constructed with uniform Φ on the domain. Indeed, the mass conservation equation leads to the fact that $K = (v - c)\rho$ is constant. The travelling waves are then constructed on the profiles of stationary solutions.

5. NUMERICAL SCHEMES

In [9], a simplified model was introduced, in which the density was assumed to be constant. In this special case, the system was reduced to a single advection–diffusion equation for the enthalpy in the following way

$$\text{Simplified model of [9]: } \begin{cases} \varrho(y, t) \text{ constant,} \\ v(y, t) = D_e/\varrho \text{ (constant),} \\ \varrho\partial_t h + D_e\partial_y h - \partial_{yy}\mathcal{L}(h) = \Phi. \end{cases} \quad (5.1)$$

An implicit scheme was introduced for this simplified model and the convergence toward the steady state solution was illustrated.

In the present paper, we tackle the complete problem (2.4). The main difference with the simplified model lies in the necessity of working under a conservative form. Indeed, the steady state solution exhibits a jump in h , leading to a jump in $h \mapsto \varrho(h)$, and thus a jump in the velocity, since $v = D_e/\varrho(h)$. As a consequence, *we cannot work with the non-conservative form as in the simplified model*. In other words, we cannot expand the products and we need to derive numerical schemes based on the conservative form.

5.1. Discretisation choices

Let us denote δt the time step and δy the space step. For any function $\star(t, y)$, let us denote \star_i^n the approximation of \star at the node i and time t^n .

5.1.1. Spatial discretisation

Let us observe that in the case of a multidimensional Stefan problem, a finite volume scheme [17] extended to a gradient scheme in [24] associated to an implicit time discretization is a key point to prove the weak convergence of the discrete solution in an $L_{t,y}^2$ norm. Indeed, it is important to discretize the diffusion term in a consistent way under the form $\partial_{yy}(\mathcal{L}(h))$, so that we avoid the ambiguous form $\partial_y(\lambda_\kappa\partial_y h)$, where λ_κ has to be defined on the grid.

For the generalized Stefan problem studied here, we also choose a gradient scheme and focus on the discrete jump relation at gas transition. We choose an upwind discretization of the convection terms (here v is always

positive) and a centered discretization of diffusion:

$$\begin{aligned}\partial_y(\varrho v) &= \frac{(\varrho v)_i - (\varrho v)_{i-1}}{\delta y}, & \partial_y(\varrho h v) &= \frac{(\varrho h v)_i - (\varrho h v)_{i-1}}{\delta y}, \\ \partial_{yy}(\mathcal{L}(h)) &= \frac{\mathcal{L}(h_{i+1}) - 2\mathcal{L}(h_i) + \mathcal{L}(h_{i-1}))}{(\delta y)^2}.\end{aligned}$$

5.1.2. Time discretisation

Let us discuss the possible time discretisations for the system (2.4). More precisely, given h^n and v^n , we want to compute h^{n+1} and v^{n+1} .

First, observe that *full explicit schemes* are prohibited in low Mach number models (with or without thermal diffusion), since there is no explicit time derivative of v in the equations (the system is not hyperbolic). With the following discretisation

$$\begin{cases} \frac{\varrho^{n+1} - \varrho^n}{\delta t} + \partial_y(\varrho v)^n = 0, \\ \frac{(\varrho h)^{n+1} - (\varrho h)^n}{\delta t} i + \partial_y(\varrho h v)^n - \partial_{yy}(\mathcal{L}(h^n)) = \Phi, \end{cases}$$

h^{n+1} (or ϱ^{n+1}) is overdetermined (by both equations), but v^{n+1} is not determined by any of the equations.

Further, in the case of explicit discretisations, a natural approach is to consider *explicit predictor-corrector schemes*, meaning that one equation is used to compute a prediction of one variable, which is then used in the second equation in order to deduce the second variable.

In any case, observe that since the solutions we want to capture numerically present possible jumps, we need to construct schemes from the conservative formulation of the equations. Thus, contrary to Navier–Stokes or usual low Mach number models (such as the LMNC model without diffusion), schemes based on the non-conservative form are not suitable with diffusion. Moreover, in the second equation of (2.4), both the diffusion and the transport terms have to be discretized at the same time. Indeed, because of the possible jumps of the solution, each of these two terms can present a jump, and these two jumps have to compensate each other at each time step.

Furthermore, notice that the second equation of (2.4) cannot be used to compute h^{n+1} . Indeed, depending on the equation of state $\varrho(h)$, the function $h \mapsto \varrho(h)h$ can be non-invertible, thus the quantity h^{n+1} cannot be deduced from $(\varrho h)^{n+1}$. It is in particular the case for the stiffened gas equation of state, where $\varrho(h) = \zeta/(h - q)$. Specifically, with the physical values of the parameters for water (given in a non-dimensional form as in Appendix C), the function $h \mapsto \varrho(h)h$ is indeed not invertible in the range $[0.001\varrho_g^s, 1.1\varrho_\ell^s]$. We also remark that the second equation of (2.4), which involves the diffusion term (acting on the variable h), gives the evolution of ϱh (which is possibly non monotone in h). Therefore, one has to be cautious when handling this equation, *e.g.* to determine the stability condition of the scheme or to prevent possible antidiffusion.

Gathering all these observations, we conclude that we have to prevent making a prediction on ϱh . An improved approach consists in reformulating the system, which overcomes the non-invertibility of the function $h \mapsto \varrho(h)h$. Let $Q > 0$ be a constant to be fixed later. We introduce the function $\mathcal{R}(\varrho) = Q\varrho - \varrho h(\varrho)$, which is, in the case of a stiffened gas law with the parameters for water, monotone decreasing and thus invertible when choosing $Q > q_g$. Thus, we combine the first equation of (2.4) multiplied by Q with the second equation, which leads to the following equivalent system

$$\begin{cases} \partial_t \varrho + \partial_y(\varrho v) = 0, \\ \partial_t \mathcal{R} + \partial_y(\mathcal{R}v) + \partial_{yy}\mathcal{L}(h) = -\Phi. \end{cases}$$

Observe that the constant Q has to be chosen of the same order of magnitude as h , in order to avoid giving too much weight to one of the two equations. With this system, we can apply a predictor–corrector approach, with the possible choice of which equation is used for predicting which variable. Let us describe the approach we chose.

1. *Predictor step.* Consider that the values at time t^n are known: h_i^n , $\varrho_i^n \stackrel{\text{def}}{=} \varrho(h_i^n)$, $\mathcal{R}_i^n \stackrel{\text{def}}{=} \mathcal{R}(\varrho_i^n)$, v_i^n . Let us compute a prediction of \mathcal{R}_i^{n+1} by solving the following equation:

$$\frac{\mathcal{R}_i^{n+1} - \mathcal{R}_i^n}{\delta t} + \frac{(\mathcal{R}v)_i^n - (\mathcal{R}v)_{i-1}^n}{\delta y} + \frac{\mathcal{L}(h_{i+1}^n) - 2\mathcal{L}(h_i^n) + \mathcal{L}(h_{i-1}^n)}{(\delta y)^2} = -\Phi. \quad (5.2a)$$

We deduce the density ϱ_i^{n+1} by inverting $\mathcal{R}(\varrho_i^{n+1}) = \mathcal{R}_i^{n+1}$, and we finally obtain the enthalpy h_i^{n+1} by solving $\varrho(h_i^{n+1}) = \varrho_i^{n+1}$.

2. *Corrector step.* We now compute the value of the velocity v^{n+1} using the new value of ϱ_i^{n+1} by solving the equation:

$$\frac{\varrho_i^{n+1} - \varrho_i^n}{\delta t} + \frac{\varrho_i^{n+1} v_i^{n+1} - \varrho_{i-1}^{n+1} v_{i-1}^{n+1}}{\delta y} = 0, \quad (5.2b)$$

with the boundary condition $v_0^{n+1} = v_e(t^{n+1})$.

With this choice, observe that the stability condition could be inferred from the prediction step in each phase (liquid, mixture, gas). Since the diffusion term of this equation is nonlinear in h and explicit, the CFL condition is not straightforward to derive, but the time step is quadratic in δy , which is very restrictive and motivates the investigation of a full implicit approach.

We can write a *full implicit scheme* in the following way. For known values at time t^n h_i^n , ϱ_i^n , v_i^n , we compute $\{h_i^{n+1}\}_i$ and $\{v_i^{n+1}\}_i$ solutions of the linear system

$$\begin{cases} \frac{\varrho_i^{n+1} - \varrho_i^n}{\delta t} + \frac{(\varrho v)_i^{n+1} - (\varrho v)_{i-1}^{n+1}}{\delta y} = 0, \\ \frac{(\varrho h)_i^{n+1} - (\varrho h)_i^n}{\delta t} + \frac{(\varrho h v)_i^{n+1} - (\varrho h v)_{i-1}^{n+1}}{\delta y} - \frac{\mathcal{L}(h_{i+1}^{n+1}) - 2\mathcal{L}(h_i^{n+1}) + \mathcal{L}(h_{i-1}^{n+1})}{(\delta y)^2} = \Phi. \end{cases} \quad (5.3)$$

This scheme does not require any CFL condition, but it requires to solve a nonlinear system at each time step. We use a Newton algorithm, and adapt the time step at each iteration in order to ensure the convergence of the algorithm.

5.2. Discrete jump relations

In this paragraph, we will describe the discrete jump relations satisfied by the two different schemes we proposed (either explicit or implicit), in the case when h is an increasing function of y .

Let us denote the discrete jumps at the interface at node i as $\llbracket \star \rrbracket_{i,j} \stackrel{\text{def}}{=} \star_i - \star_{i-j}$.

Proposition 5.1 (Mixture/Gas transition - Implicit scheme). *Assume that there exists an index i such that*

$$h_\ell^s < h_{i-2}^{n+1} \leq h_{i-1}^{n+1} < h_g^s \leq h_i^{n+1},$$

i.e. h_{i-2}^{n+1} and h_{i-1}^{n+1} are in the mixture phase and h_i^{n+1} is in the gas phase. For the implicit scheme (5.3), the jump relations at the transition point are written

$$0 = -c_\varrho [[\varrho]]_{i,2}^{n+1} + [[\varrho v]]_{i,2}^{n+1}, \quad (5.4)$$

$$2\Phi\delta y = -c_{\varrho h} [[\varrho h]]_{i,2}^{n+1} + [[\varrho h v]]_{i,2}^{n+1} - \lambda_g s_g, \quad (5.5)$$

where we introduced the discrete displacement velocities of the interface

$$c_\varrho \stackrel{\text{def}}{=} -\frac{(\varrho_{i-1}^{n+1} - \varrho_{i-1}^n) + (\varrho_i^{n+1} - \varrho_i^n) \delta y}{[[\varrho]]_{i,2}^{n+1} \delta t}, \quad (5.6)$$

$$c_{\varrho h} \stackrel{\text{def}}{=} -\frac{((\varrho h)_{i-1}^{n+1} - (\varrho h)_{i-1}^n) + ((\varrho h)_i^{n+1} - (\varrho h)_i^n) \delta y}{[[\varrho h]]_{i,2}^{n+1} \delta t}, \quad (5.7)$$

and the discrete slope of enthalpy in the gas region at the interface

$$s_g \stackrel{\text{def}}{=} \frac{h_{i+1}^{n+1} - h_i^{n+1}}{\delta y}.$$

Observe that these jump relations mimic the continuous ones (4.1).

Proof. First, consider the scheme written for the steady state equation. By summing the discretized equation at the nodes i and at node $i - 1$, it yields to

$$\begin{cases} [[\varrho v]]_{i,2} = 0, \\ [[\varrho h v]]_{i,2} - \lambda_g s_g = 2\Phi\delta y. \end{cases}$$

For unsteady flows, let us sum the discretized mass conservation equation at the nodes i and $i - 1$ to obtain directly the first jump relation. Considering now the second discretized conservation equation at the same nodes leads to

$$\begin{aligned} 2\Phi\delta y &= -c_{\varrho h} [[\varrho h]]_{i,2}^{n+1} + [[\varrho h v]]_{i,2}^{n+1} - \frac{\mathcal{L}(h_{i+1}^{n+1}) - 2\mathcal{L}(h_i^{n+1}) + \mathcal{L}(h_{i-1}^{n+1})}{\delta y} - \frac{\mathcal{L}(h_i^{n+1}) - 2\mathcal{L}(h_{i-1}^{n+1}) + \mathcal{L}(h_{i-2}^{n+1})}{\delta y} \\ &= -c_{\varrho h} [[\varrho h]]_{i,2}^{n+1} + [[\varrho h v]]_{i,2}^{n+1} - \frac{\mathcal{L}(h_{i+1}^{n+1}) - \mathcal{L}(h_i^{n+1}) - \mathcal{L}(h_{i-1}^{n+1}) + \mathcal{L}(h_{i-2}^{n+1})}{\delta y}. \end{aligned}$$

Since $h_\ell^s < h_{i-2}^{n+1} \leq h_{i-1}^{n+1} < h_g^s$, $\mathcal{L}(h_{i-2}^{n+1}) = \mathcal{L}(h_{i-1}^{n+1})$ and it becomes the claimed relation. \square

Proposition 5.2 (Liquid/Gas transition - Implicit scheme). *Assume that there exists an index i such that*

$$h_{i-3}^{n+1} \leq h_{i-2}^{n+1} \leq h_\ell^s \leq h_{i-1}^{n+1} < h_g^s \leq h_i^{n+1},$$

i.e. h_{i-3}^{n+1} and h_{i-2}^{n+1} are in the liquid phase, h_{i-1}^{n+1} is in the mixture phase and h_i^{n+1} is in the gas one. For the implicit scheme (5.3), the jump relations at the transition point are written

$$0 = -c_\varrho [[\varrho]]_{i,3}^{n+1} + [[\varrho v]]_{i,3}^{n+1}, \quad (5.8)$$

$$3\Phi\delta y = -c_{\varrho h} [[\varrho h]]_{i,3}^{n+1} + [[\varrho h v]]_{i,3}^{n+1} + \lambda_\ell s_\ell - \lambda_g s_g, \quad (5.9)$$

where the displacement velocities of the interface are defined as

$$c_\varrho \stackrel{\text{def}}{=} -\frac{(\varrho_{i-2}^{n+1} - \varrho_{i-2}^n) + (\varrho_{i-1}^{n+1} - \varrho_{i-1}^n) + (\varrho_i^{n+1} - \varrho_i^n) \delta y}{[[\varrho]]_{i,3}^{n+1}} \frac{\delta y}{\delta t}, \quad (5.10)$$

$$c_{\varrho h} \stackrel{\text{def}}{=} -\frac{((\varrho h)_{i-2}^{n+1} - (\varrho h)_{i-2}^n) + ((\varrho h)_{i-1}^{n+1} - (\varrho h)_{i-1}^n) + ((\varrho h)_i^{n+1} - (\varrho h)_i^n) \delta y}{[[\varrho h]]_{i,3}^{n+1}} \frac{\delta y}{\delta t}, \quad (5.11)$$

and the discrete slope of enthalpy in the liquid region at the interface is given by

$$s_\ell \stackrel{\text{def}}{=} \frac{h_{i-2}^{n+1} - h_{i-3}^{n+1}}{\delta y}.$$

The jump relations again mimic the continuous ones (4.2).

Proof. Consider again the scheme written for the steady equation. By summing the discretized equation at node i , at node $i-1$ and at node $i-2$, it yields to

$$\begin{cases} [[\varrho v]]_{i,3} = 0, \\ [[\varrho h v]]_{i,3} + \lambda_\ell s_\ell - \lambda_g s_g = 3\Phi \delta y. \end{cases}$$

For unsteady flows, let us sum the discretized mass conservation equation at the nodes i , $i-1$ and $i-2$ to obtain directly the first jump relation. For the second one, the same technique leads to

$$\begin{aligned} 3\Phi \delta y &= -c_{\varrho h} [[\varrho h]]_{i,3}^{n+1} + [[\varrho h v]]_{i,3}^{n+1} - \frac{\mathcal{L}(h_{i+1}^{n+1}) - 2\mathcal{L}(h_i^{n+1}) + \mathcal{L}(h_{i-1}^{n+1})}{\delta y} \\ &\quad - \frac{\mathcal{L}(h_i^{n+1}) - 2\mathcal{L}(h_{i-1}^{n+1}) + \mathcal{L}(h_{i-2}^{n+1})}{\delta y} - \frac{\mathcal{L}(h_{i-1}^{n+1}) - 2\mathcal{L}(h_{i-2}^{n+1}) + \mathcal{L}(h_{i-3}^{n+1})}{\delta y} \\ &= -c_{\varrho h} [[\varrho h]]_{i,3}^{n+1} + [[\varrho h v]]_{i,3}^{n+1} - \frac{\mathcal{L}(h_{i+1}^{n+1}) - \mathcal{L}(h_i^{n+1}) - \mathcal{L}(h_{i-2}^{n+1}) + \mathcal{L}(h_{i-3}^{n+1})}{\delta y}. \end{aligned}$$

Now, since $h_{i-3}^{n+1} \leq h_{i-2}^{n+1} \leq h_\ell^s$ and $h_g^s \leq h_i^{n+1}$, we obtain the claimed relation. \square

Analogously, we can write the corresponding jump relations for the explicit scheme, with a completely similar proof.

Proposition 5.3 (Explicit scheme).

- Mixture/Gas transition. Assume that there exists an index i such that

$$h_\ell^s < h_{i-2}^n \leq h_{i-1}^n < h_g^s \leq h_i^n.$$

For the explicit scheme (5.2), the jump relations at the transition point are written

$$-2\Phi \delta y = -c_{\mathcal{R}} [[\mathcal{R}]]_{i,2}^n + [[\mathcal{R} v]]_{i,2}^n + \lambda_g s_g, \quad (5.12)$$

$$0 = -c_\varrho [[\varrho]]_{i,2}^{n+1} + [[\varrho v]]_{i,2}^{n+1}, \quad (5.13)$$

where c_ϱ is defined in (5.6) and we introduced the displacement velocity of the interface

$$c_{\mathcal{R}} \stackrel{\text{def}}{=} -\frac{(\mathcal{R}_{i-1}^{n+1} - \mathcal{R}_{i-1}^n) + (\mathcal{R}_i^{n+1} - \mathcal{R}_i^n) \delta y}{\llbracket \mathcal{R} \rrbracket_{i,2}^n} \frac{\delta y}{\delta t}, \quad (5.14)$$

and the discrete slope of enthalpy in the gas region at the interface

$$s_g \stackrel{\text{def}}{=} \frac{h_{i+1}^n - h_i^n}{\delta y}.$$

- Liquid/Gas transition. Assume that there exists an index i such that

$$h_{i-3}^n \leq h_{i-2}^n \leq h_\ell^s < h_{i-1}^n < h_g^s \leq h_i^n.$$

For the explicit scheme, the jump relations at the transition point are written

$$-3\Phi\delta y = -c_{\mathcal{R}} \llbracket \mathcal{R} \rrbracket_{i,3}^n + \llbracket \mathcal{R}v \rrbracket_{i,3}^n + \lambda_g s_g - \lambda_\ell s_\ell, \quad (5.15)$$

$$0 = -c_\varrho \llbracket \varrho \rrbracket_{i,3}^{n+1} + \llbracket \varrho v \rrbracket_{i,3}^{n+1}, \quad (5.16)$$

where c_ϱ is defined in (5.10) and we introduced the displacement velocity of the interface

$$c_{\mathcal{R}} \stackrel{\text{def}}{=} -\frac{(\mathcal{R}_{i-2}^{n+1} - \mathcal{R}_{i-2}^n) + (\mathcal{R}_{i-1}^{n+1} - \mathcal{R}_{i-1}^n) + (\mathcal{R}_i^{n+1} - \mathcal{R}_i^n) \delta y}{\llbracket \mathcal{R} \rrbracket_{i,3}^n} \frac{\delta y}{\delta t}, \quad (5.17)$$

where the discrete slope of enthalpy in the liquid region at the interface is given by

$$s_\ell \stackrel{\text{def}}{=} \frac{h_{i-2}^n - h_{i-3}^n}{\delta y}.$$

Remark 5.4 (Possible compensation of the jump size with the interface velocity). The unsteady discrete jump relations mimic the continuous ones at order 1. Thus, the accuracy of the jump size ensures the accuracy of the interface velocities. *A contrario*, satisfying these jump relations, any inaccuracy on the jump size induces inaccuracy of the interface velocity (and reciprocally).

Remark 5.5. Observe that the works in [17, 24] investigate the generalized Stefan and prove the $L_{t,y}^2$ convergence of the solution, which ensures the correct position of the jump over time under the assumptions that the solution is monotone in space and non-oscillating in time. Although the discrete jump relation does not prove the convergence of the jump size and its velocity over time, this information complements such an $L_{t,y}^2$ convergence.

In Propositions 5.1, 5.2, and 5.3, the existence and uniqueness of the index i that defines the liquid/gas or mixture/gas transition node are guaranteed, provided the enthalpy is monotone in space and crosses the phase change thresholds. Let us comment on this monotony property. First, for the stationary equation, the explicit solution given in Propositions 3.3 and 3.5 is indeed increasing, and both schemes (explicit via a predictor–corrector approach and implicit) preserve this monotony property (this is a particular case of the proof of Appendix B). As for the transient regime, we can prove that the enthalpy solution to the equations is monotone in each phase. Thus, if assuming that the phases are ordered from liquid to gas from left to right, this is sufficient to prove the monotony. At the discrete level, we do not recover this property on the full model, but we observe it numerically. Finally, in the case of the simplified model, the monotony can be proved for the explicit scheme (see Appendix B).

Remark 5.6. Let us note that any global increase in the order of the scheme fails due to oscillations at the discontinuity point. However, in regions where the solution is continuous, classical order-increasing methods could be applied.

6. NUMERICAL VALIDATION

In the following we consider the Stiffened Gas (SG) equation of state, in which the density in each phase κ is given as a function of the enthalpy by

$$\varrho_\kappa(h) = \frac{\zeta_\kappa}{h - q_\kappa}.$$

The dimensionless values of the parameters ζ_κ , q_κ and h_κ^s are given in Table C.1(B) in Appendix C. As it is discussed in the Appendix, in the test cases, the important quantities leading to different possible behaviors are the ratios r_ℓ , r_g and r_Φ defined in (3.2). In our numerical tests, we modify the values of these ratios to illustrate the effects of diffusion and energy deposition under all possible configurations.

6.1. Validation of the implicit scheme on the travelling wave solution

In this subsection, we shall consider different configurations, for which we can exhibit a travelling wave solution (*cf.* Prop. 4.3) and check the behavior of the numerical scheme. These different configurations correspond to the different cases in Proposition 4.3, depending if the mixture phase exists or not. More precisely, the three test cases are the following, for the ratios defined in Lemma 4.2:

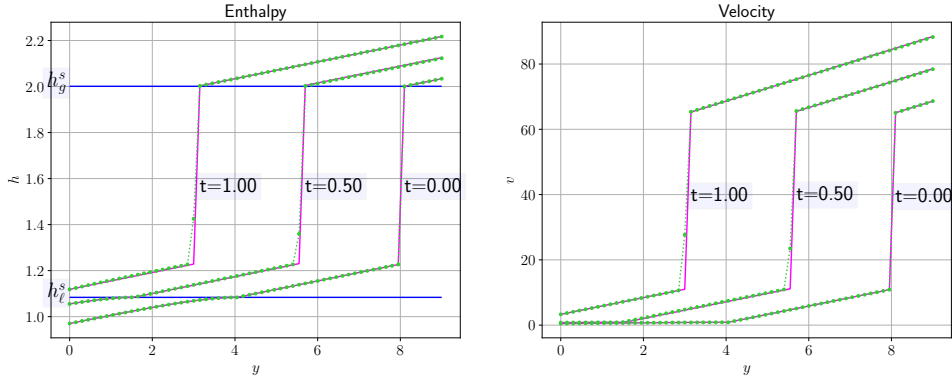
- ① the three phases coexist (liquid–mixture–gas); for this case, we choose $r_\ell = 0.966\,457$, $r_g = 20.9846$, $r_\Phi = 0.036\,635\,8$;
- ② the mixture phase disappears in the critical case when the slope of the enthalpy at the liquid–gas transition point is zero; for this case, we choose $r_\ell = 0.966\,457$, $r_g = 25.0346$, $r_\Phi = 0.036\,635\,8$;
- ③ the mixture phase disappears and the slope of the enthalpy at the transition point is positive; for this case, we choose $r_\ell = 0.845\,65$, $r_g = 29.8609$, $r_\Phi = 0.032\,056\,3$.

In each case, the travelling wave velocity is set to $c = -5$, and the final time is set to $t_{\text{final}} = 1$, while the size of the domain is $L = 9$. The different test cases are run with the implicit scheme (5.3), on a coarse grid with $N = 61$ points so that $\delta y = 0.15$.

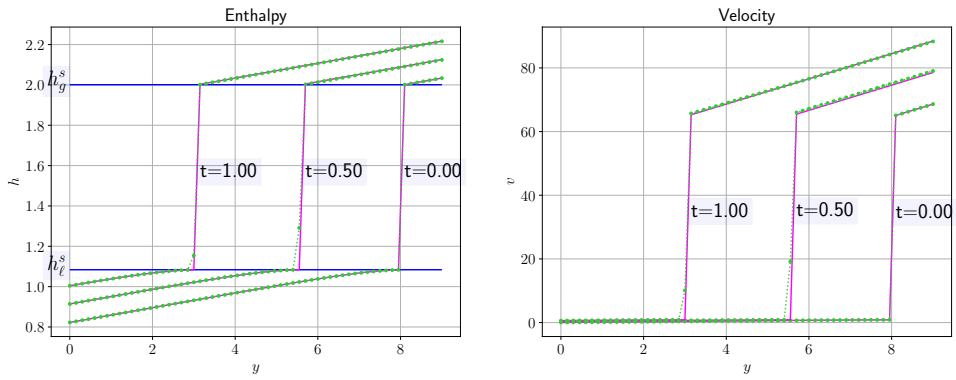
As mentioned previously, the implicit scheme has an adaptive time step at each iteration, based on the convergence of the Newton algorithm. In the simulations, the variation of the time step does not happen very often, and the time step remains of the same order of magnitude during the whole simulation. The order of magnitude of the time step can be chosen either quite large (with respect to the transport scale) or quite small. However, choosing a large time step increases the number of iterations of the Newton algorithm, thus to a reduction of the time step and no gain in the execution time. As an example, if we choose the order of magnitude of the time step to be around a tenth of the order of the transport scale, *i.e.* $\delta t = 0.1\delta y / \max_i(|v_i|)$, the Newton algorithm needs on average 2.45 iterations to converge at each time step for the test case ③. This is the choice that has been made initially for all test cases, and it does not vary much along the simulations.

We observe on Figure 4 that the numerical scheme is able to approximate very precisely the travelling wave solution for the three test cases. In each case, and at each time, only one grid point is in the jump, and the position of the profile fits the exact one within one grid point.

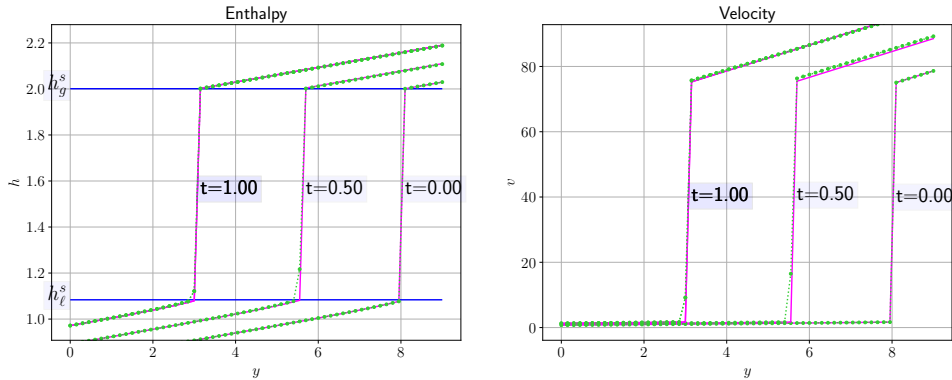
In order to assess the quality of the approximation of the displacement velocity of the jump, we plot on Figure 5(A) the exact travelling wave velocity ($c = -5$) as well as the two numerical displacement velocities of the mixture–gas interface c_g and c_{gh} defined by (5.6). We observe that the two velocities are very close to each other and oscillate around their mean values (in time), which are very close to the exact velocity c . The standard deviation of these oscillations is about 0.18. However, we notice that these oscillations do not affect the precision on the position of the jump. On Figure 5(B), we plot the error on the numerical interface position (computed



(A) Test case ①

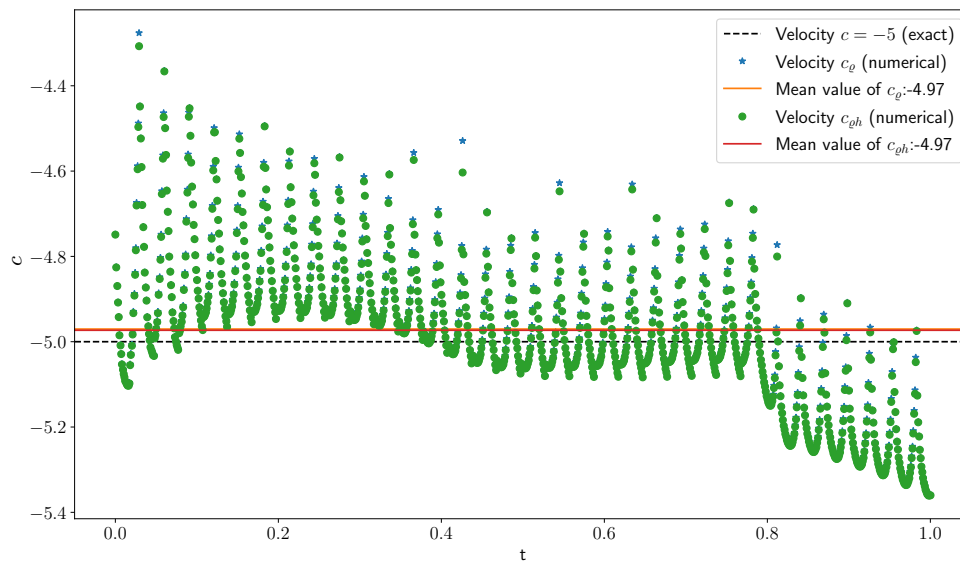


(B) Test case ②

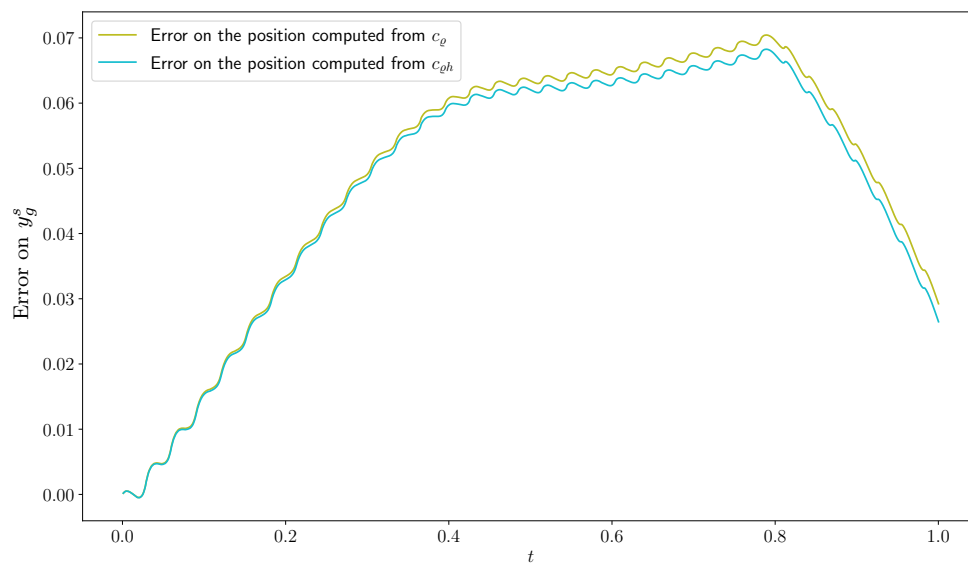


(C) Test case ③

FIGURE 4. travelling wave solution approximated with the implicit scheme for the test cases ①, ②, ③. For each test case, the enthalpy is displayed on the left, and the velocity on the right, at three different times ($t = 0$, $t = 0.5$, $t = 1$). The exact solution is the magenta continuous line, the numerical solution is the green dashed one.



(A) Exact and numerical displacement velocities of the mixture-gas interface



(B) Error on the interface position integrated from the numerical displacement velocities

FIGURE 5. Displacement of the jump for the test case ①.

by direct integration of both c_ℓ and c_{gh}) with respect to its exact value (integration of the exact displacement velocity) along time. The error does not exceed half of the mesh size (error under 0.07, with $\delta y = 0.15$).

6.2. Appearance of phases and convergence towards the asymptotic solution

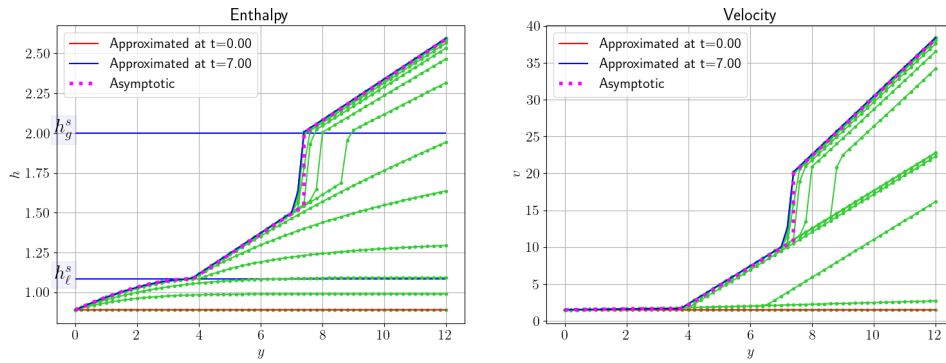
In this subsection, we consider a constant initial enthalpy corresponding to the liquid phase. The energy deposit through heating increases the enthalpy along the time and phase changes occur. We focus on three different test cases, described below:

- ④ Coexistence of the three phases (liquid–mixture–gas) in the asymptotic solution; for this case, we choose $r_\ell = 3.3826$, $r_g = 3.55272$, $r_\Phi = 0.128225$, and the boundary condition on the enthalpy is equal to $h_e = 0.889189$; the solution will be plotted for several times $t = 7j/14$, with $j = 0, \dots, 14$, which allows to see the transient behavior;
- ⑤ Disappearance of the mixture phase in the asymptotic solution, with a zero slope of the enthalpy at the liquid–gas transition point; for this case, we choose $r_\ell = 3.3826$, $r_g = 7.1527$, $r_\Phi = 0.128225$, and the boundary condition on the enthalpy is equal to $h_e = 0.922775$; the solution will be plotted for $t = j$, with $j = 0, \dots, 40$;
- ⑥ Disappearance of the mixture phase in the asymptotic solution, with a positive slope of the enthalpy at the transition point; for this case, we choose $r_\ell = 3.3826$, $r_g = 9.29855$, $r_\Phi = 0.128225$, and the boundary condition on the enthalpy is equal to $h_e = 0.814$; the solution will be plotted for $t = j$, with $j = 0, \dots, 40$.

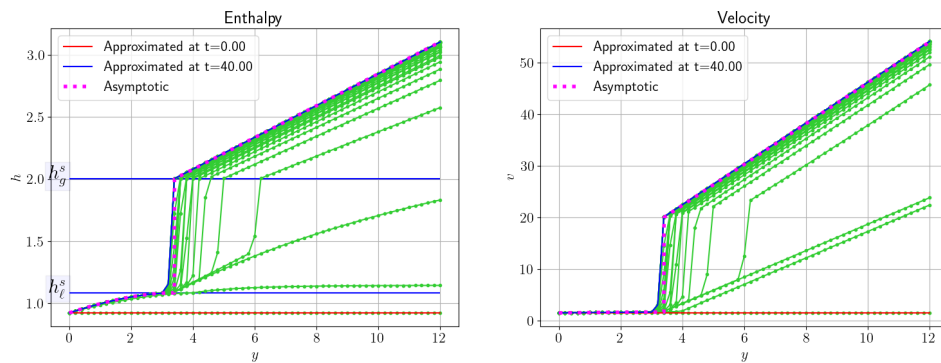
We use again the implicit scheme (5.3) on a domain of size $L = 12$, with a coarse grid consisting of $N = 61$ points, so that $\delta y = 0.2$. In all test cases, the boundary condition on the flux is set equal to $D_e = 20$, and the initial condition on the enthalpy chosen equal to the boundary condition, meaning that $h(0, y) = h_e < h_\ell^*$. For the velocity, the initial condition is set to $v(0, y) = \frac{D_e}{g(h_e)}$ to satisfy the coupled system.

The results are plotted on Figure 6. The horizontal red lines represent the initial condition, which corresponds to a domain filled with the liquid phase. The magenta line represents the exact asymptotic solution, which is reached after a certain time. The green curves show the transient regime at different times. The transition points are clearly visible, and the position of the jump is well approximated by the numerical scheme. The convergence of the solution towards the asymptotic one is also visible, as the green curves tend to the magenta one. We also emphasize the approximated curve at the final time in blue, which is very close to the asymptotic solution, except for one grid point in the jump. Let us mention three main aspects of the unsteady solution.

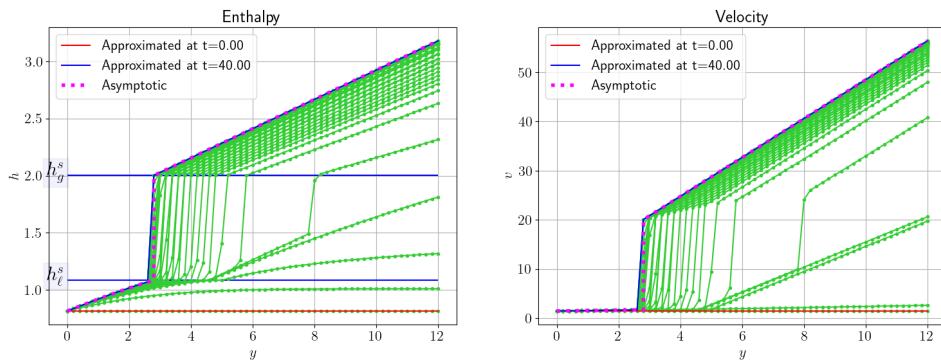
- *Transient behavior richness.* At the beginning of the simulation, the whole domain is filled with water (red lines). The green curves for the first two times correspond to a pure liquid flow. After a while, the heating causes the appearance of the mixture, then followed by the appearance of the gas phase. As soon as the gas appears, a jump (inside the mixture phase) gradually grows, simultaneously reducing the mixture region. In the cases ⑤ and ⑥, the mixture phase completely disappears. Between these two cases, we see that the slope of the enthalpy at the transition point differs.
- *Accuracy of the scheme.* We show on Figure 7 the results for the same test cases, but with a refined grid consisting of $N = 961$ points (so that $\delta y = 0.0125$). We observe that the solution is very close to the asymptotic one, with only one grid point in the jump. This confirms the convergence of the scheme towards the exact solution, as the grid is refined. We also observe that the transition points are well approximated, and the position of the jump is very close to the exact one. We quantified this convergence by computing the relative error in the L^∞ norm on the flow rate at the final time, with respect to the exact asymptotic one which is constant equal to D_e . As an example, for the test ④, the error is 1.75×10^{-2} with $N = 61$, and 5.67×10^{-3} with $N = 961$.
- *Grid convergence.* In order to show the convergence of the scheme on the grid, we define a reference solution computed on a very fine grid with $N = 961$ points (so that $\delta y = 0.0125$). Let us denote by h_{ref} and v_{ref} the enthalpy and velocity of this reference solution. We focus on the same time instants $(t_j)_{0 \leq j \leq J}$ as for Figure 6 ($J = 14$ for the test case ④, $J = 40$ for the test cases ⑤ and ⑥). We then compare the solution



(A) Test case ④



(B) Test case ⑤



(C) Test case ⑥

FIGURE 6. Unsteady solution approximated with the implicit scheme with a coarse grid consisting of $N = 61$ points. For each test case, the enthalpy is displayed on the left, and the velocity on the right, at different times with green lines. The initial solution is the red line, the exact asymptotic solution is the magenta continuous line, the asymptotic numerical one is the blue one.

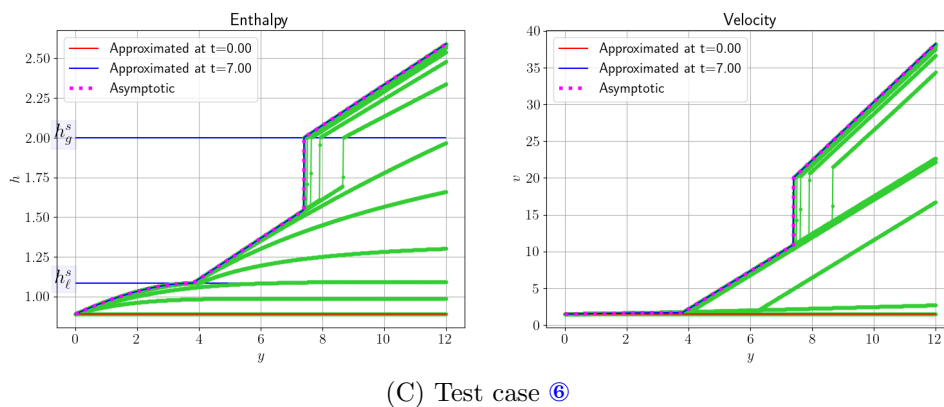
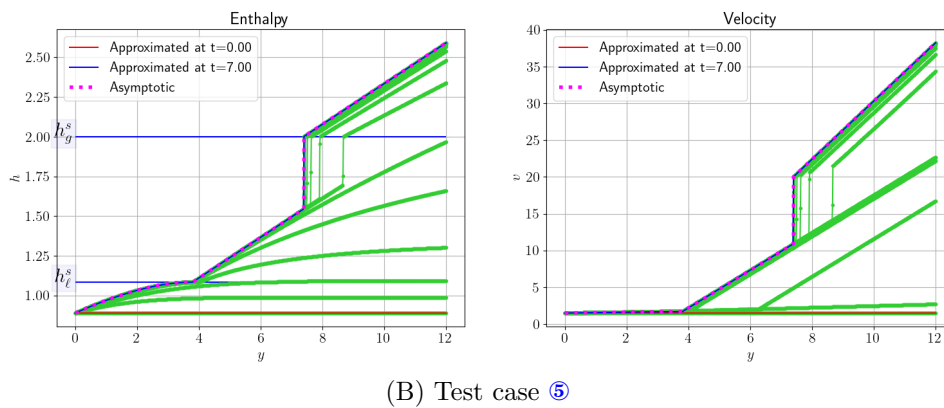
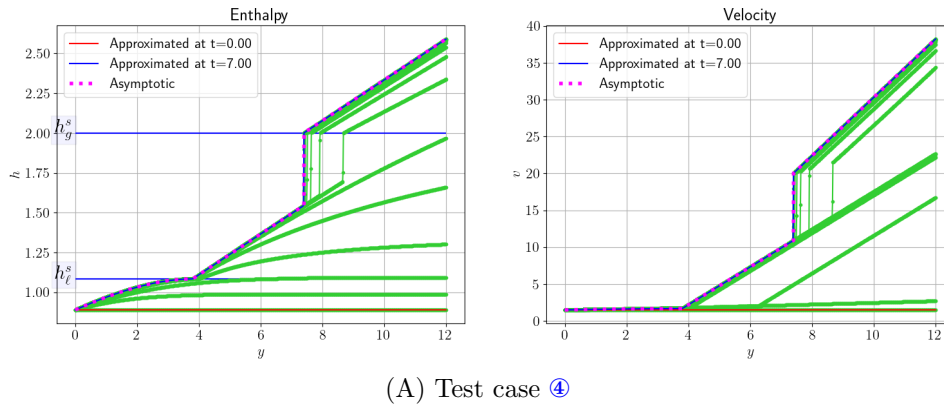


FIGURE 7. Unsteady solution approximated with the implicit scheme with a raffined grid consisting of $N = 961$ points. For each test case, the enthalpy is displayed on the left, and the velocity on the right, at different times with green lines. The initial solution is the red line, the exact asymptotic solution is the magenta continuous line, the asymptotic numerical one is the blue one.

TABLE 1. Relative $L_{x,t}^2$ error on the enthalpy and the velocity for different refinement levels.

	Test ④		Test ⑤		Test ⑥	
	\mathcal{E}_h	\mathcal{E}_v	\mathcal{E}_h	\mathcal{E}_v	\mathcal{E}_h	\mathcal{E}_v
$\delta y = 0.05$	8.321×10^{-3}	2.819×10^{-2}	1.561×10^{-2}	2.185×10^{-2}	1.036×10^{-2}	1.781×10^{-2}
$\delta y = 0.025$	3.876×10^{-3}	9.057×10^{-3}	8.071×10^{-3}	1.128×10^{-2}	5.115×10^{-3}	9.555×10^{-3}

TABLE 2. L^1 error on the transition points positions for different refinement levels.

	Test ④		Test ⑤		Test ⑥	
	\mathcal{E}_ℓ^s	\mathcal{E}_g^s	\mathcal{E}_ℓ^s	\mathcal{E}_g^s	\mathcal{E}_ℓ^s	\mathcal{E}_g^s
$\delta y = 0.05$	6.607×10^{-2}	2.250×10^{-2}	1.799×10^{-2}	1.667×10^{-2}	2.156×10^{-2}	2.566×10^{-2}
$\delta y = 0.025$	1.429×10^{-2}	1.000×10^{-2}	5.183×10^{-3}	6.410×10^{-3}	7.187×10^{-3}	9.868×10^{-3}

computed on two coarser grids, with $N = 481$ points (so that $\delta y = 0.025$) and $N = 241$ points (so that $\delta y = 0.05$), to this reference solution. We compute \mathcal{E}_h and \mathcal{E}_v the relative discrete $L_{x,t}^2$ -norm (evaluated at the times t_j) of the difference between the numerical solution and the reference one, for both the enthalpy and the velocity. The results are displayed in Table 1, where we observe that the error decreases with the grid refinement.

Further, we focus on the phase transition points, defined as follows: at each time t , $y_\ell^s(t)$ is the first mesh point at which the enthalpy is in the mixture phase, and $y_g^s(t)$ is the first mesh point at which the enthalpy is in the gas phase. To quantify the space convergence of these transition points, we compute the normalized discrete $L^1(0, T)$ error \mathcal{E}_κ^s on their positions $\frac{1}{J} \sum_{j=1}^J (y_\kappa^s(t_j) - y_{\kappa, \text{ref}}^s(t_j))$ for two different refinement levels, $\delta y = 0.05$ and $\delta y = 0.025$. The results are displayed in Table 2, where we observe that the error decreases with the grid refinement.

Additionally, we compare the transition points positions at the same instants for different refinement levels on Figure 8. We display the positions at the same time instants as in Figure 6. For any refinement level, the position of the transition points is very precise (see Fig. 8), since these points are located at the same position up to the mesh size δy . For the test case ④, which has both transition points (liquid–mixture and mixture–gas), these transition points of course only exist after some time corresponding to the appearance of the phases. For the test case ⑥, in which the mixture disappears, the two values $y_\ell^s(t)$ and $y_g^s(t)$ converge to the same one, with possibly one mesh point difference.

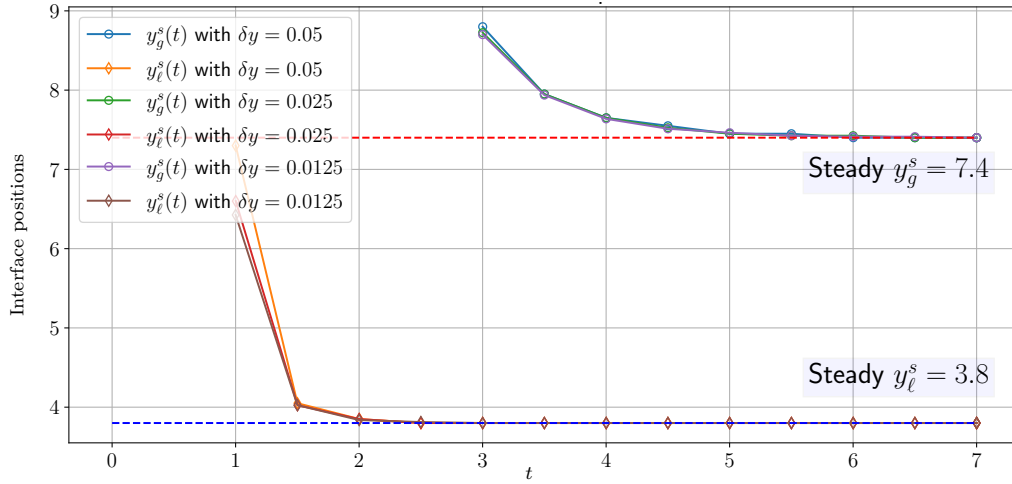
6.3. Comparison of the explicit scheme with the implicit one

The good properties of the implicit scheme have been proved in the previous section, both in the case of a travelling wave and in terms of convergence towards the exact steady solution (with phase appearance and disappearance). Thus, we choose this scheme as the reference one.

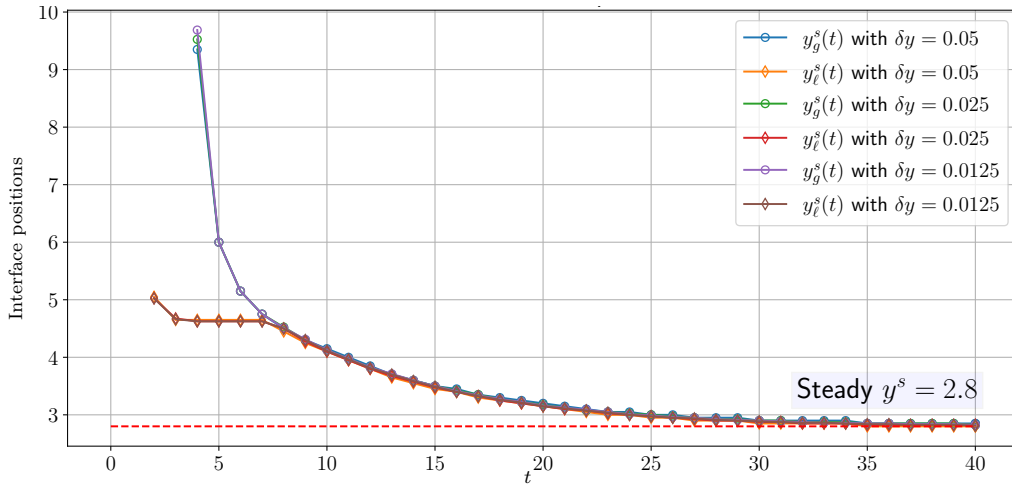
Since the explicit predictor-corrector scheme requires a restrictive CFL condition, it is only tested on coarse grids. The results are compared to the exact solution (for travelling waves) or to the solution provided by the implicit scheme.

The time step of the explicit scheme is chosen according to the following CFL condition with $C = 0.9$, which takes into account both the transport and diffusion terms in each phase:

$$\delta t = C \frac{\delta y}{\max_i \left(|v_i| + 2 \frac{\lambda_i}{\delta y \rho_i} \right)}.$$



(A) Test case ④



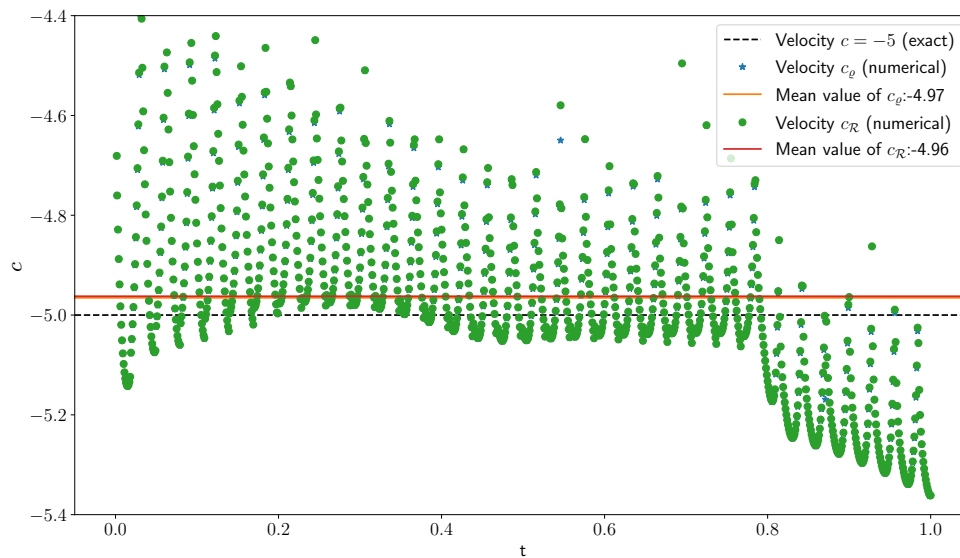
(B) Test case ⑥

FIGURE 8. Position of the phase transition points along time for different refinement levels.

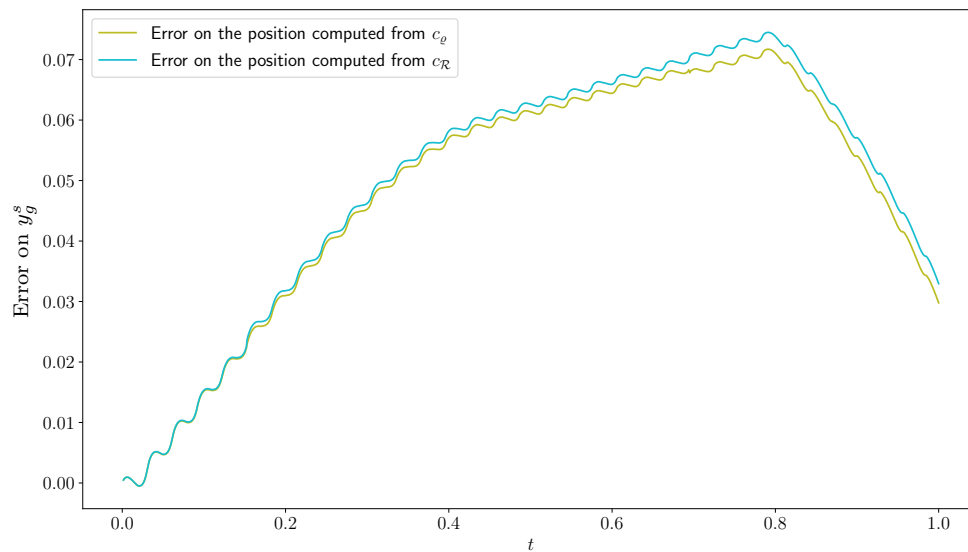
With $C = 2$, we observe the instability of the scheme, which confirms the necessity of a diffusion-like CFL condition, quadratic with the mesh size.

6.3.1. Travelling wave solution

To validate the explicit scheme, we first consider the travelling wave solution. As in Figure 5 for the implicit scheme, we display on Figure 9 the displacement of the jump for test case ① on a coarse grid. Although the two figures are not completely identical, the two schemes indeed have the same behavior, leading in particular to the same mean values of the displacement velocities of the jump (mixture–gas interface). The error on the interface position are of the same order of magnitude, in spite of a slightly higher error for the implicit scheme.



(A) Exact and numerical displacement velocities of the mixture-gas interface



(B) Error on the interface position integrated from the numerical displacement velocities

FIGURE 9. Displacement of the jump for the test case ① with the explicit scheme.

TABLE 3. Relative L^2 -errors.

	$t \approx 2.5$	$t \approx 4$	$t \approx 5.5$	$t \approx 7$		$t \approx 2.5$	$t \approx 4$	$t \approx 5.5$	$t \approx 7$
$N = 61$	0.0321	0.0322	0.0225	0.0214	$N = 61$	0.0419	0.0067	0.0007	0.0004
$N = 121$	0.0135	0.0181	0.0123	0.0138	$N = 121$	0.0205	0.0027	0.0002	0.0002
(A) Relative L^2 -error on h.					(B) Relative L^2 -error on the flow rate ρv .				

6.3.2. Appearance of phases and convergence toward the asymptotic solution

For the test case ④, we provide in Tables 3(A) and 3(B) the relative L^2 -error between the implicit and the explicit schemes on the enthalpy and the velocity at four different times ($t \approx 2.5$, $t \approx 4$, $t \approx 5.5$, $t \approx 7$) for a coarse grid with $N = 61$ points, as well as with a slightly finer grid with $N = 121$ points.

We observe that the explicit scheme behaves as the implicit one in the transient and asymptotic regime, on the different grids. The same behavior has also been observed for the other test cases.

7. CONCLUSION AND PERSPECTIVES

For the 1D LMNC model with phase change and degenerate thermal diffusion, we investigated stationary and travelling wave solutions of the model. We implemented two types of schemes (implicit and explicit), which capture correctly the discontinuities at the phase transition boundaries. Discrete jump relations are analogous to those for the continuous model. In transient regimes, we showed the good performance of the schemes in a variety of situations: appearance/disappearance of mixture, accurate phase displacement, appropriate displacement velocity and amplitude of enthalpy jumps at the gas interface. The good performance of both schemes leads us to favor the implicit scheme, which does not suffer from a restrictive CFL condition.

In a multi-dimensional context, the extension of this work is not trivial, since the equation for pressure is no longer a post-processing step. Consequently, we have a Navier–Stokes-like equation to address under a conservative form. This shall be the subject of a future work.

ACKNOWLEDGMENTS

This work has been achieved within the framework of the M2SIR project, financially supported by CNRS AAP “NEEDS 2020”, and its partners Andra, BRGM, CEA, EDF, Framatome, IRSN et Orano.

DATA AVAILABILITY STATEMENT

The data that support the findings of this study are available from the corresponding author, upon reasonable request.

REFERENCES

- [1] J.M. Delhaye, *Thermohydraulique des réacteurs*. EDP Sciences (2008).
- [2] S. Dellacherie, On a low Mach nuclear core model. *ESAIM Proc.* **35** (2012) 79–106.
- [3] S.L. Passman, J.W. Nunziato and E.K. Walsh, A Theory of Multiphase Mixtures, in *Rational Thermodynamics*. Springer, New York (1984) 286–325.
- [4] N.E. Todreas and M.S. Kazimi, *Nuclear Systems I: Thermal Hydraulic Fundamentals*, Vol. 2. Taylor & Francis (1990).
- [5] H.B. Callen, *Thermodynamics and an Introduction to Thermostatistics*, 2nd edn. John Wiley & sons (1985).
- [6] W. Greiner, L. Neise and H. Stöcker, *Thermodynamics and Statistical Mechanics*. Springer (1997).
- [7] M. Bernard, S. Dellacherie, G. Faccanoni, B. Grec and Y. Penel, Study of a low Mach nuclear core model for two-phase flows with phase transition. I: stiffened gas law. *ESAIM: Math. Model. Numer. Anal.* **48** (2014) 1639–1679.
- [8] A. Bondesan, S. Dellacherie, H. Hivert, J. Jung, V. Lleras, C. Mietka and Y. Penel, Study of a depressurisation process at low Mach number in a nuclear reactor core. *ESAIM Proc. Surv.* **55** (2016) 41–60.

- [9] G. Faccanoni and C. Galusinski, Influence of a nonlinear degenerate diffusion on an advection-diffusion equation in a diffuse interface framework. *ESAIM Proc. Surv.* **72** (2023) 143–162.
- [10] G. Faccanoni, C. Galusinski and L. Lamerand, Thermal diffusion and phase change in a heat exchanger, in *Topical Problems of Fluid Mechanics 2021*. Institute of Thermomechanics of the Czech Academy of Sciences (2021) 56–64.
- [11] J. Stefan, Über die Theorie der Eisbildung, insbesondere über die Eisbildung im Polarmeere. *Ann. Phys.* **278** (1891) 269–286.
- [12] S.C. Gupta, The Classical Stefan Problem: Basic Concepts, Modelling and Analysis. North-Holland Series in Applied Mathematics and Mechanics. *Elsevier Science* (2003).
- [13] L.I. Rubinstein, *The Stefan Problem*, vol. 8. American Mathematical Society (2000).
- [14] A. Friedman, The Stefan problem in several space variables. *Trans. Am. Math. Soc.* **133** (1968) 51–87.
- [15] O.A. Oleinik, A method of solution of the general Stefan problem, in *Doklady Akademii Nauk*, vol. 135. Russian Academy of Sciences (1960) 1054–1057.
- [16] J. Carrillo, Entropy solutions for nonlinear degenerate problems. *Arch. Rational Mech. Anal.* **147** (1999) 269–361.
- [17] R. Eymard, Th. Gallouët, R. Herbin and A. Michel, Convergence of a finite volume scheme for nonlinear degenerate parabolic equations. *Numer. Math.* **92** (2002) 41–82.
- [18] L.A. Richards, Capillary conduction of liquids through porous mediums. *Physics* **1** (1931) 318–333.
- [19] G. Faccanoni, B. Grec and Y. Penel, A homogeneous relaxation low Mach number model. *ESAIM Math. Model. Numer. Anal.* **55** (2021) 1569–1598.
- [20] A.E. Berger, H. Brezis and J.C.W. Rogers, A numerical method for solving the problem. *RAIRO Anal. Numer.* **13** (1979) 297–312.
- [21] R. Eymard, Th. Gallouët, D. Hilhorst and Y.N. Slimane, Finite volumes and nonlinear diffusion equations. *ESAIM Math. Model. Numer. Anal.* **32** (1998) 747–761.
- [22] J. Bruining, D. Marchesin and C.J. Van Duijn, Steam injection into water-saturated porous rock. *Computat. Appl. Math.* **22** (2003) 359–395.
- [23] R. Eymard and E. Tillier, Mathematical and numerical study of a system of conservation laws. *J. Evol. Equ.* **7** (2007) 197–239.
- [24] R. Eymard, P. Féron, Th. Gallouët, R. Herbin and C. Guichard, Gradient schemes for the Stefan problem. *Int. J. Finite Vol.* **10** (2013) 1–37.
- [25] Y. Penel, *Étude théorique et numérique de la déformation d'une interface séparant deux fluides non-miscibles à bas nombre de Mach*. PhD thesis, Université Paris-Nord - Paris XIII (2010).
- [26] S. Evje and K.H. Karlsen, Discrete approximations of BV solutions to doubly nonlinear degenerate parabolic equations. *Numer. Math.* **86** (2000) 377–417.
- [27] C. Cancès and C. Guichard, Convergence of a nonlinear entropy diminishing control volume finite element scheme for solving anisotropic degenerate parabolic equations. *Math. Computat.* **85** (2016) 549–580.
- [28] W. Wagner and H.-J. Kretzschmar, Tables of the properties of water and steam. International Steam Tables: Properties of Water and Steam Based on the Industrial Formulation IAPWS-IF97 (2008) 169–343.



Please help to maintain this journal in open access!

This journal is currently published in open access under the Subscribe to Open model (S2O). We are thankful to our subscribers and supporters for making it possible to publish this journal in open access in the current year, free of charge for authors and readers.

Check with your library that it subscribes to the journal, or consider making a personal donation to the S2O programme by contacting subscribers@edpsciences.org.

More information, including a list of supporters and financial transparency reports, is available at <https://edpsciences.org/en/subscribe-to-open-s2o>.

APPENDIX A. DERIVATION OF THE CONSERVATIVE LOW MACH NUMBER MODEL WITH THERMAL DIFFUSION

This section introduces a model designed for a heat exchanger system in the low Mach number asymptotic limit, derived from the compressible Navier-Stokes-Fourier system. For the sake of simplicity, this is done in a 1D setting. This system includes conservation equations for mass, momentum, and energy, involving the following unknowns: the velocity field $(t, y) \mapsto v$, the enthalpy $(t, y) \mapsto h$, and the pressure $(t, y) \mapsto p$, where t is the time and y the 1D space variable. It is given by the conservation equations for

$$\text{mass} \quad \partial_t \varrho + \partial_y(\varrho v) = 0, \quad (\text{A.1})$$

$$\text{momentum} \quad \partial_t(\varrho v) + \partial_y(\varrho v^2 + p) = -\varrho g + \partial_y \sigma, \quad (\text{A.2})$$

$$\text{energy} \quad \partial_t E + \partial_y((E + p)v) = \Phi + \partial_y(\omega \partial_y T) + \partial_y(\sigma v) - \varrho g v. \quad (\text{A.3})$$

The heating is represented by the power density $\Phi \geq 0$, and viscous effects are described by the stress tensor $\sigma = \mu \partial_y v$, where μ is the viscosity of the fluid. Other parameters are the heat conductivity ω and the gravitation g , which is opposite to the flow. An Equation of State (EoS) defining the density and the temperature as functions of the enthalpy and the pressure is needed to close the system.

We consider this model on a semi-infinite domain \mathbb{R}^+ . Dirichlet boundary conditions at the inlet $y = 0$ are imposed on the velocity $v(0, t) = v_e(t)$, on the enthalpy $h(0, t) = h_e(t)$, and on the pressure $p(0, t) = p_e$ (constant).

The energy E is linked to the enthalpy h through the thermodynamic relation $E = \frac{1}{2} \varrho v^2 + \varrho h - p$, so that (A.3) can be rewritten as

$$\partial_t(\varrho h) + \partial_y(\varrho h v) + \frac{1}{2} (\partial_t(\varrho v^2) + \partial_y(\varrho v^3)) = \partial_t p + \Phi + \partial_y(\omega \partial_y T) + \partial_y(\sigma v) - \varrho g v. \quad (\text{A.4})$$

It has to be noted that the system has to be written under a conservative form, since we shall see that in our setting, some quantities are discontinuous. Therefore, the adimensionalization of the system which has been done in the literature [2, 25] cannot be used directly, and has to be redone under a conservative form. Let us briefly describe this dimensionalization process.

First, let us define a characteristic length L_\circ , a characteristic time t_\circ and the characteristic velocity $v_\circ = L_\circ/t_\circ$, as well as a characteristic value ϱ_\circ for the density. Let us denote by $\bar{t} = t/t_\circ$, $\bar{y} = y/L_\circ$, $\bar{\varrho} = \varrho/\varrho_\circ$ and $\bar{v} = v/v_\circ$ the dimensionless quantities for time, space, density and velocity. The adimensionalization of (A.1) and division by ϱ_\circ/t_\circ leads to the same equation on the dimensionless quantities, since $v_\circ = L_\circ/t_\circ$:

$$\partial_{\bar{t}} \bar{\varrho} + \partial_{\bar{y}}(\bar{\varrho} \bar{v}) = 0. \quad (\text{A.5})$$

Further, introducing a characteristic value p_\circ for the pressure and μ_\circ for the viscosity, and the corresponding dimensionless values $\bar{p} = p/p_\circ$ and $\bar{\mu} = \mu/\mu_\circ$, the adimensionalization of (A.2) leads to the following equation on the dimensionless quantities, since $\sigma = \mu \partial_y v$:

$$\varrho_\circ v_\circ \left(\frac{1}{t_\circ} \partial_{\bar{t}}(\bar{\varrho} \bar{v}) + \frac{v_\circ}{L_\circ} \partial_{\bar{y}}(\bar{\varrho} \bar{v}^2) \right) + \frac{p_\circ}{L_\circ} \partial_{\bar{y}} \bar{p} = -\varrho_\circ g \bar{\varrho} + \frac{\mu_\circ v_\circ}{L_\circ^2} \partial_{\bar{y}}(\bar{\mu} \partial_{\bar{y}} \bar{v}).$$

Dividing by $\varrho_\circ v_\circ^2/L_\circ$ (and using that $t_\circ = L_\circ/v_\circ$), we introduce the following dimensionless numbers (resp. the Mach, the Froude and the Reynolds numbers)

$$\text{Ma} = \frac{\sqrt{\varrho_\circ} v_\circ}{\sqrt{p_\circ}}, \quad \text{Fr} = \frac{v_\circ^2}{L_\circ g}, \quad \text{Re} = \frac{\varrho_\circ v_\circ L_\circ}{\mu_\circ},$$

and obtain the adimensional equation

$$\partial_{\bar{t}}(\bar{\varrho} \bar{v}) + \partial_{\bar{y}}(\bar{\varrho} \bar{v}^2) + \frac{1}{\text{Ma}^2} \partial_{\bar{y}} \bar{p} = -\frac{1}{\text{Fr}} \bar{\varrho} + \frac{1}{\text{Re}} \partial_{\bar{y}}(\bar{\mu} \partial_{\bar{y}} \bar{v}). \quad (\text{A.6})$$

Finally, introducing characteristic values h_o for the enthalpy, T_o for the temperature, and ω_o for the heat conductivity, as well as the dimensionless values $\bar{h} = h/h_o$, $\bar{T} = T/T_o$ and $\bar{\omega} = \omega/\omega_o$, the adimensionalization of (A.4) leads to the following equation on the dimensionless quantities:

$$\begin{aligned} \varrho_o h_o \left(\frac{1}{t_o} \partial_{\bar{t}}(\bar{\varrho}\bar{h}) + \frac{v_o}{L_o} \partial_{\bar{y}}(\bar{\varrho}\bar{h}\bar{v}) \right) + \frac{1}{2} \varrho_o v_o^2 \left(\frac{1}{t_o} \partial_{\bar{t}}(\bar{\varrho}\bar{v}^2) + \frac{v_o}{L_o} \partial_{\bar{y}}(\bar{\varrho}\bar{v}^3) \right) \\ = \Phi + \frac{\omega_o T_o}{L_o^2} \partial_{\bar{y}}(\bar{\omega} \partial_{\bar{y}} \bar{T}) + \frac{p_o}{t_o} \partial_{\bar{t}} \bar{p} + \frac{\mu_o v_o^2}{L_o^2} \partial_{\bar{y}}(\bar{v} \bar{\mu} \partial_{\bar{y}} \bar{v}) - \varrho_o g v_o \bar{\varrho} \bar{v}. \end{aligned}$$

Dividing by $\varrho_o h_o v_o / L_o$, and introducing $\bar{\Phi} = \Phi t_o / (\varrho_o h_o)$, we obtain the adimensional equation

$$\begin{aligned} \partial_{\bar{t}}(\bar{\varrho}\bar{h}) + \partial_{\bar{y}}(\bar{\varrho}\bar{h}\bar{v}) + \frac{1}{2} \frac{v_o^2}{h_o} (\partial_{\bar{t}}(\bar{\varrho}\bar{v}^2) + \partial_{\bar{y}}(\bar{\varrho}\bar{v}^3)) \\ = \bar{\Phi} + \frac{\omega_o T_o}{v_o L_o \varrho_o h_o} \partial_{\bar{y}}(\bar{\omega} \partial_{\bar{y}} \bar{T}) + \frac{p_o}{\varrho_o h_o} \partial_{\bar{t}} \bar{p} + \frac{\mu_o v_o}{\varrho_o L_o h_o} \partial_{\bar{y}}(\bar{\mu} \bar{v} \partial_{\bar{y}} \bar{v}) - \frac{L_o g}{h_o} \bar{\varrho} \bar{v}. \end{aligned}$$

Introducing the dimensionless number (Prandtl number)

$$\text{Pr} = \frac{\mu_o h_o}{\omega_o T_o},$$

and assuming that $h_o = p_o / \varrho_o$, the adimensional equation becomes

$$\partial_{\bar{t}}(\bar{\varrho}\bar{h}) + \partial_{\bar{y}}(\bar{\varrho}\bar{h}\bar{v}) + \frac{1}{2} \text{Ma}^2 (\partial_{\bar{t}}(\bar{\varrho}\bar{v}^2) + \partial_{\bar{y}}(\bar{\varrho}\bar{v}^3)) = \bar{\Phi} + \frac{1}{\text{Re}} \frac{1}{\text{Pr}} \partial_{\bar{y}}(\bar{\omega} \partial_{\bar{y}} \bar{T}) + \partial_{\bar{t}} \bar{p} + \frac{\text{Ma}^2}{\text{Re}} \partial_{\bar{y}}(\bar{\mu} \bar{v} \partial_{\bar{y}} \bar{v}) - \frac{\text{Ma}^2}{\text{Fr}} \bar{\varrho} \bar{v}. \quad (\text{A.7})$$

Then, for performing the asymptotic limit in the low Mach number regime, in a similar way to what has been done in the literature, all quantities are expanded as power series of the Mach number, all other dimensionless numbers being assumed to be of order 1 (actually, the Reynolds and Froude numbers can be chosen such as $1/\text{Re} = o(1)$, $1/\text{Fr} = o(1)$). Let us define

$$\bar{p} = \bar{p}^{(0)} + \text{Ma} \bar{p}^{(1)} + \text{Ma}^2 \bar{p}^{(2)} + o(\text{Ma}^2),$$

and similar expansions for the other quantities. Equation (A.5) obviously does not change at the leading order

$$\partial_{\bar{t}} \bar{\varrho}^{(0)} + \partial_{\bar{y}}(\bar{\varrho}^{(0)} \bar{v}^{(0)}) = 0.$$

The two leading orders Ma^{-2} and Ma^{-1} of (A.6) give that

$$\partial_{\bar{y}} \bar{p}^{(0)} = \partial_{\bar{y}} \bar{p}^{(1)} = 0,$$

and the equation at order Ma^0 becomes

$$\partial_{\bar{t}}(\bar{\varrho}^{(0)} \bar{v}^{(0)}) + \partial_{\bar{y}}(\bar{\varrho}^{(0)} (\bar{v}^{(0)})^2) + \partial_{\bar{y}} \bar{p}^{(2)} = -\frac{1}{\text{Fr}} \bar{\varrho}^{(0)} + \frac{1}{\text{Re}} \partial_{\bar{y}}(\bar{\mu} \bar{v} \bar{v}^{(0)}). \quad (\text{A.8})$$

Moreover, choosing the boundary condition p_e independent of t implies that $\bar{p}^{(0)}$ is independent of \bar{t} , and thus constant, and $\bar{p}^{(1)}$ is zero. Equation (A.7) then becomes at order Ma^0

$$\partial_{\bar{t}}(\bar{\varrho}^{(0)} \bar{h}^{(0)}) + \partial_{\bar{y}}(\bar{\varrho}^{(0)} \bar{h}^{(0)} \bar{v}^{(0)}) = \bar{\Phi} + \frac{1}{\text{Re}} \frac{1}{\text{Pr}} \partial_{\bar{y}}(\bar{\omega} \partial_{\bar{y}} \bar{T}^{(0)}). \quad (\text{A.9})$$

Observe that this asymptotic procedure uncouples the pressure as the sum of a reference constant pressure $\bar{p}_* \stackrel{\text{def}}{=} \bar{p}^{(0)}$ at order Ma^0 and a perturbational pressure $\bar{\mathcal{P}}(t, y) \stackrel{\text{def}}{=} \bar{p}^{(2)}$ at order Ma^2 , which becomes the new unknown of the system. Moreover, this formulation simplifies the equation of state, since the density and the temperature now only depend on one variable, the enthalpy, because the pressure involved in the thermodynamic functions is constant.

The equation of state on the temperature gives the function $T(h)$. Since the thermal diffusion term involves $\bar{\omega}(\bar{h}^{(0)})\partial_{\bar{y}}\bar{T}(\bar{h}^{(0)})$, let us define the function $\bar{\mathcal{L}}(\bar{h})$ such that

$$\bar{\mathcal{L}}'(\bar{h}) \stackrel{\text{def}}{=} \bar{\omega}(\bar{h})\bar{T}'(\bar{h}). \quad (\text{A.10})$$

In this way, the thermal diffusion term can be rewritten as $\partial_{\bar{y}\bar{y}}\bar{\mathcal{L}}(\bar{h}^{(0)})$. Observe that when $\bar{T}'(\bar{h}) = 0$, $\bar{\mathcal{L}}'(\bar{h}) = 0$. When $\bar{T}'(\bar{h}) \neq 0$, introducing the isobaric heat capacity $c_p(h) = \frac{\partial h}{\partial T}|_p$, and the dimensionless value $\bar{c}_p(\bar{h}) = c_p(h)T_o/h_o$, we can define

$$\bar{\lambda}(\bar{h}) \stackrel{\text{def}}{=} \bar{\omega}(\bar{h})/\bar{c}_p(\bar{h}). \quad (\text{A.11})$$

If we set $\bar{\lambda}(\bar{h}) = 0$ when $\bar{T}'(\bar{h}) = 0$, the function $\bar{\mathcal{L}}$ satisfies $\bar{\mathcal{L}}'(\bar{h}^{(0)}) = \bar{\lambda}(\bar{h}^{(0)})$.

We now have the complete set of dimensionless equations:

$$\begin{cases} \partial_{\bar{t}}\bar{\rho}^{(0)} + \partial_{\bar{y}}(\bar{\rho}^{(0)}\bar{v}^{(0)}) = 0 \\ \partial_{\bar{t}}(\bar{\rho}^{(0)}\bar{v}^{(0)}) + \partial_{\bar{y}}(\bar{\rho}^{(0)}(\bar{v}^{(0)})^2) + \partial_{\bar{y}}\bar{\mathcal{P}} = -\frac{1}{\text{Fr}}\bar{\rho}^{(0)} + \frac{1}{\text{Re}}\partial_{\bar{y}}(\bar{\mu}\partial_{\bar{y}}\bar{v}^{(0)}) \\ \partial_{\bar{t}}(\bar{\rho}^{(0)}\bar{h}^{(0)}) + \partial_{\bar{y}}(\bar{\rho}^{(0)}\bar{h}^{(0)}\bar{v}^{(0)}) = \bar{\Phi} + \frac{1}{\text{Re}}\frac{1}{\text{Pr}}\partial_{\bar{y}\bar{y}}(\bar{\mathcal{L}}(\bar{h}^{(0)})) \end{cases} \quad (\text{A.12})$$

For the sake of clarity, throughout this paper, we consider dimensionless quantities at the leading order in the Mach number expansion, omitting the bar notation and corresponding superscripts, which turns (A.12) into

$$\begin{cases} \partial_t \rho(h) + \partial_y(\rho(h)v) = 0 \\ \partial_t(\rho(h)v) + \partial_y(\rho(h)v^2) + \partial_y \mathcal{P} = -\frac{1}{\text{Fr}}\rho(h) + \frac{1}{\text{Re}}\partial_y(\mu\partial_y v) \\ \partial_t(\rho(h)h) + \partial_y(\rho(h)hv) = \Phi + \frac{1}{\text{Re}}\frac{1}{\text{Pr}}\partial_{yy}(\mathcal{L}(h)). \end{cases} \quad (\text{A.13})$$

A.1 Adimensionalisation of the Equation of State

The equation of state also has to be adimensionalized. We choose here the piecewise Stiffened Gas (SG) equation of state for each pure phase. In the mixture, the equation of state also has the form of a SG (*cf.* [7] when coupled with the LMNC model). The equation of state is given piecewise by (2.2). At constant pressure p_* , we have

$$\begin{aligned} \rho_\kappa(h) &\stackrel{\text{def}}{=} \frac{\zeta_\kappa}{h - q_\kappa}, \quad \kappa \in \{\ell, m, g\}; \\ T_\kappa(h) &\stackrel{\text{def}}{=} \frac{h - q_\kappa}{c_{p,\kappa}} \quad \kappa \in \{\ell, g\}, \quad \text{and} \quad T(h) = T^s \quad \text{in the mixture.} \end{aligned}$$

By introducing the dimensionless values $\bar{\zeta}_\kappa = \zeta_\kappa/(h_o\rho_o)$, $\bar{q}_\kappa = q_\kappa/h_o$, $\bar{c}_{p,\kappa} = c_{p,\kappa}T_o/h_o$, we define

$$\bar{\rho}_\kappa(\bar{h}) = \frac{\bar{\zeta}_\kappa}{\bar{h} - \bar{q}_\kappa}, \quad \bar{T}_\kappa(\bar{h}) = \frac{\bar{h} - \bar{q}_\kappa}{\bar{c}_{p,\kappa}},$$

so that $\bar{\rho}(\bar{h})$ and $\bar{T}(\bar{h})$ are defined piecewise using $\bar{\rho}_\kappa(\bar{h})$ and $\bar{T}_\kappa(\bar{h})$, depending on the value of \bar{h} with respect to $\bar{h}_\ell^s = h_\ell^s/h_o$ and $\bar{h}_g^s = h_g^s/h_o$. Analogously, $\bar{\zeta}(\bar{h})$, $\bar{\omega}(\bar{h})$ and $\bar{c}_p(\bar{h})$ are defined piecewise on the same intervals, which defines $\bar{\lambda}(\bar{h})$ as

follows

$$\bar{\lambda}(\bar{h}) = \begin{cases} \bar{\lambda}_\ell \stackrel{\text{def}}{=} \bar{\omega}_\ell / \bar{c}_{p,\ell} & \text{if } \bar{h} < \bar{h}_\ell^s, \\ 0 & \text{if } \bar{h}_\ell^s < \bar{h} < \bar{h}_g^s, \\ \bar{\lambda}_g \stackrel{\text{def}}{=} \bar{\omega}_g / \bar{c}_{p,g} & \text{if } \bar{h} > \bar{h}_g^s. \end{cases} \quad (\text{A.14})$$

APPENDIX B. DISCRETE MONOTONY OF THE SOLUTION FOR THE SIMPLIFIED MODEL

In the following proposition, we prove that the explicit numerical scheme preserves the monotony of the solution h for the simplified model (5.1) (which uncouples the two equations *via* a constant density). Note that this simplified model is related to the class of models studied in [26], where the convergence of the numerical scheme to the unique BV entropy solution is established. We obtain supplementary information on the monotony of the solution for the simplified model in the following proposition.

Proposition B.1. *Assume that the equation of state leads to a constant density, i.e. let us consider the simplified model (5.1), approached with the explicit scheme. If the initial enthalpy $y \mapsto h_0(y)$ is increasing, then the discrete enthalpy remains increasing at each time steps under the CFL-like condition*

$$\delta t \leq \frac{1}{\frac{v}{\delta y} + \frac{2C_{\mathcal{L}}}{\rho\delta y^2}},$$

where $C_{\mathcal{L}} = \max(\lambda_\ell, \lambda_g)$ is the Lipschitz constant of the function \mathcal{L} .

Proof. Let us denote

$$\partial_i^+ \star \stackrel{\text{def}}{=} \frac{\star_{i+1} - \star_i}{\delta y}, \quad \partial_i^- \star \stackrel{\text{def}}{=} \frac{\star_i - \star_{i-1}}{\delta y}.$$

In the particular case of a constant density ρ , the mass conservation leads to a constant velocity v , and the equation of enthalpy reduces to

$$\partial_t h + v \partial_y h - \frac{1}{\rho} \partial_{yy} (\mathcal{L}(h)) = \frac{\Phi}{\rho}.$$

The explicit scheme reads for any $i \in \mathbb{N}^*$

$$\frac{h_i^{n+1} - h_i^n}{\delta t} + v \partial_i^- h^n - \frac{1}{\rho} \partial_i^- \partial^+ (\mathcal{L}(h^n)) = \frac{\Phi}{\rho}, \quad (\text{B.1})$$

where $\partial^\pm \star$ is the vector whose i -th component is $\partial_i^\pm \star$. Assume that $\partial_i^- h^n \geq 0$ for all $i \in \mathbb{N}^*$. We aim to prove that $\partial_i^- h^{n+1} \geq 0$ for all $i \in \mathbb{N}^*$.

Let us define (B.1) for node $i = 0$ by introducing the corresponding h_{-1}^n . Observe that, from the boundary condition $h_0 = h_e$, (B.1) at node $i = 0$ is thus written as

$$\frac{v}{\delta y} (h_e - h_{-1}^n) - \frac{1}{\rho\delta y^2} (\mathcal{L}(h_1^n) - \mathcal{L}(h_e)) + \frac{1}{\rho\delta y^2} (\mathcal{L}(h_e) - \mathcal{L}(h_{-1}^n)) = \frac{\Phi}{\rho}.$$

We use the positivity of Φ/ρ and the fact that $\mathcal{L}(h_1^n) - \mathcal{L}(h_e) \geq 0$, to deduce

$$\frac{v}{\delta y} (h_e - h_{-1}^n) + \frac{1}{\rho\delta y^2} (\mathcal{L}(h_e) - \mathcal{L}(h_{-1}^n)) \geq 0.$$

Defining $\mathcal{G} = v + \mathcal{L}/\rho\delta y$, which is obviously increasing (as \mathcal{L} and since $v \geq 0$), we deduce that $h_{-1}^n \leq h_e$.

TABLE C.1. Values of the parameters for water at $p_* = 15.5$ MPa.

Phase	q_κ [J kg ⁻¹]	ζ_κ [Pa]	h_k^s [J kg ⁻¹]	$\lambda_k = \omega_k/c_{p,k}$ [kg s ⁻¹ m ⁻¹]
Liquid	-1.16706e+06	1.76772e+09	1.62704e+06	0.052 643 4
Mixture	1.50131e+06	7.95475e+07	N/A	N/A
Gas	2.03026e+06	5.15465e+07	3.00398e+06	0.008 961 42

(A) Values of the parameters taken from [7] for the SG EoS and from the NIST database [28] for the thermal conductivity.

Phase	\bar{q}_κ	$\bar{\zeta}_\kappa$	\bar{h}_κ^s	$\bar{\lambda}_\kappa$
Liquid	-0.777 36	22.2222	1.083 75	0.000 993 542
Mixture	1	1	N/A	0
Gas	1.35232	0.647 996	2.000 91	0.000 169 13

(B) Values of the dimensionless parameters.

The key point of the proof lies in the dominant-diagonal operators ∂^- and $-\partial^-\partial^+$ with a maximum-like principle under a restrictive condition on the time step. Let us write the solution at time t^{n+1} as a combination of the solution at time t^n

$$h_i^{n+1} = \left(1 - \frac{v}{\delta y}\right) h_i^n - \frac{2}{\rho\delta y^2} \mathcal{L}(h_i^n) + \frac{v}{\delta y} h_{i-1}^n + \frac{1}{\rho\delta y^2} \mathcal{L}(h_{i-1}^n) + \frac{1}{\rho\delta y^2} \mathcal{L}(h_{i-1}^n).$$

For $i \geq 1$, subtracting this equation at node i and at node $i-1$, we obtain,

$$\begin{aligned} \partial_i^- h^{n+1} &= \left(1 - \frac{v\delta t}{\delta y}\right) \partial_i^- h^n - \frac{2\delta t}{\rho\delta y^2} (\mathcal{L}(h_i^n) - \mathcal{L}(h_{i-1}^n)) + \frac{v\delta t}{\delta y} \partial_{i-1}^- h^n \\ &\quad + \frac{\delta t}{\rho\delta y^2} (\mathcal{L}(h_{i-1}^n) - \mathcal{L}(h_{i-2}^n)) + \frac{\delta t}{\rho\delta y^2} (\mathcal{L}(h_{i+1}^n) - \mathcal{L}(h_i^n)). \end{aligned}$$

Using the Lipschitz property of the function \mathcal{L} , we then have,

$$\partial_i^- h^{n+1} \geq \left(1 - \frac{v\delta t}{\delta y} - \frac{2C_{\mathcal{L}}\delta t}{\rho\delta y^2}\right) \partial_i^- h^n + \frac{v\delta t}{\delta y} \partial_{i-1}^- h^n + \frac{\delta t}{\rho\delta y^2} (\mathcal{L}(h_{i-1}^n) - \mathcal{L}(h_{i-2}^n)) + \frac{\delta t}{\rho\delta y^2} (\mathcal{L}(h_{i+1}^n) - \mathcal{L}(h_i^n)).$$

From the assumption that the enthalpy at time t^n is non decreasing in space, the growth of \mathcal{L} ensures that

$$\partial_i^- h^{n+1} \geq \left(1 - \frac{v\delta t}{\delta y} - \frac{2C_{\mathcal{L}}\delta t}{\rho\delta y^2}\right) \partial_i^- h^n.$$

The right-hand side is then positive under the restrictive condition on the time step given in the Proposition. \square

Remark B.2. The key point to ensure the monotonicity of the solution is the property of diagonally dominant operators for transport and diffusion. When extended to multidimensional problems, the same property is essential. For degenerate parabolic equations, this property is fulfilled in [27] for a finite volume scheme with an upwind discretization of the flux.

APPENDIX C. VALUES OF THE PARAMETERS OF THE SG LAW IN THE CASE OF WATER

For numerical simulations, it remains to determine the reference values we mentioned. In a pressurized water reactor, which is the physical context which motivated the study of the LMNC model [7], the pressure in the core of the reactor is

about $p_* = 15.5$ MPa. At this pressure, the temperature at saturation is $T^s(p_*) = 654.651$ K. The values of the parameters of the equation of state for the case of water at this pressure are given in Table C.1(A).

Let us choose $h_o = q_m$, $\varrho_o = \zeta_m/h_o$ (*i.e.* $p_o = \zeta_m$) and $T_o = T^s(p_*)$. Further, we choose $L_o = v_o = 1$ (and thus $t_o = 1$), and ω_o such that $\text{RePr} = 1$ (*i.e.* $\omega_o = \varrho_o v_o L_o h_o / T_o = \zeta_m / T^s$). This implies that the reference value λ_o is defined by $\lambda_o = \omega_o T_o / h_o = \varrho_o v_o L_o$. The corresponding dimensionless parameters are given in Table C.1(B).

For the power density, in a pressurized water reactor (PWR), we can consider $\Phi = 1.7 \times 10^8 \text{ W m}^{-3}$, so that $\bar{\Phi} = t_o \Phi / (h_o \varrho_o) = 2.13709$. In the same physical setting, we can choose $v_e = 1 \text{ m s}^{-1}$, and $h_e = 0.5 h_\ell^s$ (ensuring that the injection is liquid). This leads to the following adimensional value of the entrance flow $\bar{\varrho}_e \bar{v}_e = 16.85$.

In Section 3, we discussed the importance of the three ratios r_ℓ , r_g and r_Φ defined in (3.2) in the analysis of the model. For example, we show that different behaviors are obtained depending on the condition $r_g r_\Phi \gtrless h_g^s - h_\ell^s$. In the case of the core of a PWR we described before, this ratio is

$$r_g r_\Phi / (h_g^s - h_\ell^s) \approx 1.3 \cdot 10^{-6}.$$

These values are very far from the equality case, for which the mixture disappears. This shows that thermal diffusion effects leading to jumps can be neglected in the physical setting and justify the approach of previous papers (*e.g.* [7, 19]).

In the numerical simulations of Section 6, we shall change artificially the ratios to show that the numerical schemes capture all the possible types of behaviors. This is physically motivated by the fact that other heat carriers are possible, and that the values of the parameters can be different. In particular, for metallic heat carriers, thermal diffusion is more important.